Quasi-Static and Dynamic Behavior of Precast Concrete Frames with High Performance Dry Connections subjected to Loss of a Penultimate Column Scenario

Kai Qian[1*], Shi-Lin Liang[1], Xue-Yu Xiong[2], Feng Fu[3], and Qin Fang[4*]

[1]College of Civil Engineering and Architecture, Guangxi University, Nanning, China, 530004.

[2] College of Civil Engineering, Tongji University, Shanghai, China, 200092.

[3] School of Mathematics, Computer Science and Engineering, City, University of London, U.K.

[4] Army Engineering University, Nanjing, Jiangsu, China, 210007.

Abstract:

Unbonded post-tensioned precast concrete (UPPC) frame exhibits excellent performance in resisting seismic load from experimental tests and post-earthquake investigations. However, the behavior of UPPC frames subjected to extreme load such as the loss of a column due to explosion is still not well studied. To fill this knowledge gap, in this paper, four 1/2 scaled UPPC beam-column substructures were tested under both quasi-static and dynamic loading regimes. The comparative study between these two test-regimes were subsequently performed, which provides a clear understanding of the difference of these two test methods in progressive collapse studies for other researchers. The test results indicated that UPPC frames achieved required load redistribution capacity to mitigate progressive collapse. The failure modes of the frames observed in dynamic test were quite similar to that in quasi-static tests. Moreover, it was found that strain rate effects were insignificant for progressive collapse events caused by suddenly column removal. Based on the measured load resisting function from quasi-static tests, a single-degree-of-freedom (SDOF) model, with the consideration of strain hardening and softening, was developed. After validation, the proposed SDOF model was used to quantify the effects of service load, initial velocity, initial displacements, and damping ratio on the dynamic response. It was found that the damping ratio， non-zero initial velocity and initial displacement are the three most influential parameters.

Keywords: Dynamic, Static and Progressive Collapse; Precast Concrete; Unbonded Posttensioned Analysis

* Corresponding author. Tel.: 86+771-3232894, E-mail address: qiankai@gxu.edu.cn

1. Introduction

Unbonded post-tensioned precast concrete (UPPC) system was first advocated in PREcast Seismic Structural System (PRESSS) program [1] due to its high-ability of self-centering and low residual deformation. Afterwards, a number of studies have been carried out to further investigate its seismic performance of UPPC system. To enhance the energy dissipation ability of UPPC system, Stone et al. [2] and Stanton et al. [3] embedded mild steel across the beam-column joints. However, this modification may lead to irreparable damage at the beam ends causing certain difficulties in construction. Therefore, extensive studies [4-10] were devoted to facilitate the reparability of the UPPC system.

Previous studies indicated that UPPC system performed well under cyclic loads. Different to seismic design, progressive collapse design focused on gravity load redistribution capacity of the structures. Moreover, the ability of developing secondary load resisting mechanism to mitigate progressive collapse requires sufficient deformation capacity and ductility. However, investigation on progressive collapse performance of UPPC system is rare. Lu et al. [11] proposed a sort of unbonded posttensioned steel-concrete composite frame for seismic and progressive collapse mitigation. The proposed frame exhibited better behavior than conventional frames in resisting either seismic loading or progressive collapse. Qian et al. [12] experimentally investigated the performance of UPPC frames with different dry connections to resist progressive collapse. They reported that compressive arch action (CAA) and tensile catenary action (TCA) could be mobilized to resist progressive collapse simultaneously. However, only quasi-static behavior was investigated and the dynamic response of UPPC frame under sudden removal of a penultimate column, which representing a typical terrorist attack or vehicular impact scenario, was in need of investigation.

As it is stipulated in DoD [13], four methods for progressive collapse analysis: linear static (LS), nonlinear static (NS), linear dynamic (LD), and nonlinear dynamic (ND) analyses can be used for progressive collapse design. LS and NS analyses are easy to perform while they fall short in capturing dynamic nature of progressive collapse. LD analysis is capable of including inertia effects while fail to account for nonlinear characteristic of the building. Therefore, ND analysis is the best option for progressive collapse analysis due to its high accuracy. However, ND analysis requires substantial computing resource which results in inconvenience in engineering application. To integrate advantages, load increase factor (LIF) and dynamic increase factor (DIF) are proposed to convert LS results and NS results to ND behavior, respectively. Relying on this, dynamic resistance could be obtained from quasi-static response. Considerable efforts have been carried out to investigate the nonlinear static response of beam-column sub-assemblages under column removal scenario through quasi-static tests. Sadek et al. [14] tested two full scaled reinforced concrete (RC) assemblies in accordance with different seismic intensity. In their tests, the decline of load resistance was measured due to concrete crushing while re-ascending of load resistance was observed owing to TCA. Moreover, the failure of the assemblies was controlled by fractured of bottom rebar near the middle column. Qian and Li [15-16] performed a series of tests to study the load redistribution capacity of RC frame subjected to the loss of a corner column. They reported that CAA and TCA were inefficient due to limited axial restraints. Yu and Tan [17] investigated the structural behavior of RC beam-column sub-assemblages under a middle column removal scenario. It was found that both CAA and TCA could be developed as long as adequate axial and rotational restraints provided. Valipour et al. [18] studied the effects of concrete strength and reinforcement ratio on behavior of RC frames to mitigate progressive collapse. The test results indicated that the relationship between CAA capacity and concrete strength is approximately linear whereas reinforcement ratio has a minor effect on the contribution of CAA. Quiel et al. [19] proposed a new type of connection for precast concrete buildings to resist progressive collapse, the connection exhibited favorable damage avoidance capacity. Meanwhile, several dynamic tests were also performed recently. Qian and Li [20-21] evaluated the dynamic performance of RC frame under the loss of a corner column by using specially designed column removal apparatus. Furthermore, DIF was quantified by comparing the dynamic response to corresponding static one. They proposed that the DIF recommended by DoD [13] for structural component with force-controlled behavior may be too conservative. Yu et al. [22] reported the dynamic progressive collapse response of RC sub-assemblages under an explosively removed column. The test results proved that the strain effects of material were insignificant. Russell et al. [23] performed static and dynamic tests to investigate the load carrying capacity of RC flat structure under different column removal scenarios (corner, penultimate or interior column). They found that the load distribution behavior obtained from dynamic tests was similar to that from static ones. They also proposed that the recommended DIF was conservative. Qian et al. [24] experimentally and numerically investigated the dynamic behavior of RC flat slab structure under two column missing scenario. The results indicated that RC flat slab structure could achieve new balance even two columns (one interior and one side column) were removed suddenly.

In addition, energy equivalent method [25] is frequently used to assess the dynamic response based on measured quasi-static load resisting function. However, this method ignores the effects of damping and thus may lead to conservative prediction. Single-degree-of-freedom (SDOF) model [26-28] is another favorable way to predict dynamic response. After conducting dynamic incremental analysis, the dynamic ultimate load (DUL) of the specimens can be obtained and therefore a force based DIF, which is defined as the ratio of static ultimate load (SUL) to the DUL, can be obtained [20].

To have a deeper understanding of the difference of static procedure and dynamic procedure stipulated in the design codes, in this paper, two UPPC frames were designed and tested under quasi-static test regime to investigate the load resisting mechanism of UPPC system subjected to the loss of a penultimate column scenario. Meanwhile, two counterparts, which have identical reinforcement details and dimensions, were tested under dynamic test regime using specially designed column removal apparatus to capture their dynamic response subjected to sudden column missing scenarios. Note that, the DUL could not be determined purely relied on these two dynamic tests. For this reason, a SDOF model was developed based on the response captured from quasi-static tests. After validation, the proposed model was employed to determine the DUL of tested dynamic specimens. Moreover, the model was used to investigate the effect of service load, non-zero initial condition, and damping ratio on dynamic response caused by sudden column missing.

2. Experimental program

2.1. Test specimens

In this study, four 1/2 scaled UPPC beam-column substructures, extracted from the prototype structure at the inflection points, were tested subjected to either quasi-static or dynamic loading regimes. The prototype structure is an eight-storey frame located on a D class site, which was designed in accordance with ACI 318-14 [29]. The design response spectrum acceleration parameters of SDS and SD1 are 0.46 and 0.29, respectively. The design live load (LL) is 2.0 kPa. The dead load (DL) including the ceiling weight is 5.1 kPa. Table 1 tabulates the characteristics of the specimens. These four specimens can be categorized into two groups (UPPC-S and UPPC-D). The quasi-static group includes UPPC-SL and UPPC-SH whereas the dynamic group has two specimens UPPC-DL and UPPC-DH. The designation “UPPC” represents Unbonded Posttensioned Precast Concrete frame. The letter “S” and “D” represent quasi-static and dynamic test, respectively. In addition, the last letter “L” and “H” denote axial compression ratio of 0.2 and 0.4 at the side column, respectively. It should be noted that all specimens have identical reinforcement detailing and dimensions. As shown in Fig. 1, the specimen consists of two beams, two side columns, one middle column stub, and an overhanging beam beyond one of the side columns as a penultimate column removal was assumed. The side column with overhanging beam represents interior side column (to simulate horizontal restraints from surrounding bays). Conversely, the side column without overhanging beam represents exterior side column where no additional horizontal restraints.

The cross-section of beam and column was 150 mm × 250 mm and 250 mm × 250 mm, respectively. The longitudinal reinforcement for column is 4T16 while the top and bottom beam were both 2T12. R6 was used as transverse reinforcements for beam and column. “T16”, “T12”, and “R6” represent deformed rebar with diameter of 16 mm, 12 mm, and plain rebar with diameter of 6 mm, respectively. Moreover, spiral hoops with diameter of 60 mm were embedded at the beam ends to enhance the concrete strength. PVC tubes with diameter of 20 mm were embedded in the precast beams and columns for assembly purpose. The beams and columns were assembled by unbonded posttensioned strands with nominal diameter and area of 12.7 mm and 98.7 mm^2, respectively.

2.2. Material properties

At the day of tests, cylinder tests indicated, the concrete compressive strength of UPPC-SL, UPPC-SH, UPPC-DL, and UPPC-DH, were 38.5 MPa, 39.4 MPa, 37.5 MPa, and 38.1 MPa, respectively. In addition, the tensile splitting tests indicated the tensile strength at the day of test is 3.7 MPa, 3.6 MPa, 3.5 MPa, and 3.8 MPa, for UPPC-SL, UPPC-SH, UPPC-DL, and UPPC-DH, respectively. The properties of the reinforcements and strands were listed in Table 2.

2.3. Test setup and instrumentations

Fig. 2 gives test setup and layout of instrumentations. For quasi-static tests, as shown in Fig. 2a, the top of side column and overhanging beam, if any, were connected to an A-frame via a roller connection while the bottom of the side column was sit on a pin support. The ground level penultimate column was removed prior to vertical load applied by a hydraulic jack (Item 1 in Fig. 2a). To prevent undesired out-of-plane failure, a steel assembly (Item 3 in Fig. 2a) was specially placed beneath the hydraulic jack (Item 1 in Fig. 2a). The axial compressive force on the side column was applied by a hydraulic jack (Item 6 in Fig. 2a) with a self-equilibrium system. To measure test results properly, extensive instrumentations were installed. A load cell (Item 2 in Fig. 2a) was installed just below the hydraulic jack (Item 1 in Fig. 2a) to measure the applied concentrated load. Tension/compression load cell (Item 5 in Fig. 2a) was installed at each roller to measure the horizontal reaction force of the roller. A load pin (Item 8 in Fig. 2a) was installed at the pin support to measure the vertical and horizontal reaction force of the pin support. Therefore, the behavior of vertical load redistribution and the varying of horizontal reaction force were monitored during test. Moreover, to monitor the varying of prestressing force of the strand, a load cell (Item 4 in Fig. 2a) was installed at the jacking end for each strand. Furthermore, a series of linear variable differential transformers (LVDTs) were installed along the beam span and column height to monitor the deformation shape of the beams and columns.

For dynamic tests, as shown in Fig. 2b, the test setup of dynamic specimens is almost similar to that of quasi static one, except the ground penultimate column was replaced by a specially designed sudden column removal device (SCRD, Item 10 in Fig. 2b). The SCRD comprised a steel column, a pin support, and a load cell, which had been used in [20]. Then, six weight blocks (Item 9 in Fig. 2b) with total weights of 8400 kg, were hung along the beam to simulate the service load (2(1.2DL+0.5LL)) required by load combination of dynamic analysis procedure stipulated by DoD [13]. After that, the SCRD was suddenly removed to replicate the sudden column removal. To monitor the variation of axial force in SCRD, a load cell (Item 11 in Fig. 2b) was installed beneath the steel column of the SCRD. Similar to static tests, the axial force of the roller and the vertical and horizontal reaction force of the pin supports and prestressing force of the strands were also measured in the dynamic tests, as shown in Fig. 2c.

3. Quasi-Static test observation and results

To facilitate readability, the nomenclature of this paper is shown in Table 3. As mentioned above, UPPC-SL and UPPC-SH were tested under quasi-static push-down loading regime. The key results such as first peak load (FPL), second peak load (SPL) and maximum horizontal compressive/tensile force on the exterior and interior side (E-MHCF/E-MHTF, I-MHCF/I-MHTF) were summarized in Table 4.

3.1. Global behavior and failure modes

Fig. 3 gives the load-middle joint displacement (MJD) curve of the specimens. The FPL of UPPC-SL and UPPC-SH is 39 kN and 41 kN, respectively. At relatively small deformation stage, the initial stiffness of UPPC-SH is slightly higher than that of UPPC-SL as the higher axial compressive ratio on side column increases the stiffness of horizontal restraints of the beams. The load resistance of UPPC-SH is greater than that of UPPC-SL until the MJD reached 530 mm. It should be pointed out that UPPC-SH reaches its SPL at MJD of 461 mm while UPPC-SL keeps increasing until reaching an MJD of 600 mm. The SPL of UPPC-SH and UPPC-SL is 78 kN and 90 kN, respectively. Therefore, larger compressive axial force on side column could increase its FPL and initial stiffness slightly, but decrease its SPL and deformation capacity significantly, which could be explained as the larger axial compressive force on side column resulted in the failure of side column earlier due to greater P-Δ effects in exterior side column.

Fig. 4 presents the failure modes of UPPC-SL. As shown in the figure, wide openings were observed at the beam-column interfaces. The damage of beam was concentrated at compressive toes while no cracks are observed along the beams during the test as the unbonded posttensioned strands induces considerable compressive stress and the beam longitudinal reinforcement is discontinuous at the beam-column interface. At the end of the test, the exterior side column (without overhanging beam) experiences a typical large eccentric compression failure. However, the interior side column is observed much milder damage: only few flexural cracks formed in the inner face of the side column. This is because the overhanging beam could provide required horizontal restraints and resulting in less P-Δ effects. In general, as shown in Fig. 5, similar phenomenon is observed for UPPC-SH. Compared to UPPC-SL, the concrete crushing of exterior side column of UPPC-SH is more severe due to greater P-Δ effects. The observation above proves that the failure modes of UPPC frames are quite different from that of RC frames [14-15, 17, 30-31] and commonly used precast concrete frames with wet or dry connections [32-35]. In these tests, plastic hinges are formed at the beam ends and penetrated cracks were formed along the beam at catenary action stage.

3.2. Deformation shape of the beam and column

Fig. 6 presents the varying of deformation shape of the double-bay beam of UPPC-SL in accordance with different MJDs. It can be found that the double-bay beams deformed in a twofold line manner during the test, which agrees well with the failure mode. Generally, similar results are measured at UPPC-SH. Fig. 7 illustrates the lateral deflection of the side column of UPPC-SH. The lateral displacement achieved negative (outward) first and then changes to positive (inward). For the exterior side column, the maximum outward and inward movements are -0.69 mm and 43.43 mm, respectively. However, they are -0.62 mm and 7.6 mm for interior side column, respectively.

3.3. Horizontal reaction force

Figs. 8a and b illustrate the distribution of horizontal reaction of UPPC-SH on exterior and interior side, respectively. Due to horizontal restraint, the outward and inward movement causes compressive (negative value) and tensile (positive value) reaction on the boundary. It can be found that column bottom restraint contributes majority of compressive reaction force on both sides whereas the contribution from top roller could be ignored maybe due to relatively large gap existed. With increased displacement, the horizontal reaction force changes from compression to tension following increased prestressing forces in strands. In tension phase, column top and bottom provide tensile reaction force almost equally for exterior side. However, the roller connected to the overhanging beam contributes majority of tensile reaction force for interior side column. Generally, similar phenomenon is measured at UPPC-SL. Table 4 tabulates the maximum horizontal reaction of the specimens. For UPPC-SL, the E-MHCF, I-MHCF, E-MHTF, and I-MHTF are -62 kN, -75 kN, 135 kN and 259 kN, respectively. However, they are -67 kN, -84 kN, 156 kN, and 253 kN for UPPC-SH, respectively. It proves that the interior side experiences larger reaction in both tension and compression phase due to stronger restraints.

3.4. Bending moment in the exterior side column

To further reveal the failure mode of exterior side column, the variation of bending moment of the exterior side column was illustrated in Fig. 9. As shown in the inserted figure, the bending moment in section E-E can be determined by Eq. 1:

$$M_E = H_1 l_0 + V_1 \Delta \qquad (1)$$

where H_1 is the horizontal reaction force from top roller; l_0 is the distance from top roller to section E-E; V_1 is the axial compressive force on the exterior side column; Δ is horizontal drift in section E-E.

As shown in Fig. 9, the bending moment is negative at small deformation stage due to compressive horizontal reaction force from top roller, whereas it changes to positive at large deformation stage because the horizontal reaction force changes from negative to positive. Fig. 10 gives the theoretical bending moment-axial force curve of E-E section and the points represent the measured axial force and maximum bending moment of the section. As the points located at the portion of tensile failure, it agrees with the failure mode of the exterior side column well (large eccentric compressive failure).

3.5. Load resisting mechanism

Due to special configuration, the load resisting mechanisms mobilized in UPPC frame are significantly different to that in RC frames [12]. For RC frames, flexural action (FA), CAA and TCA will be mobilized in sequence to mitigate collapse. For UPPC frames, as illustrated in Fig. 11, FA will not develop due to limited rotational restraint at the beam end. CAA relies on the arching force (N in the figure) in beam which is induced by prestressing force in the strands and axial restraint. Moreover, the TCA due to tensioning of the strands is mobilized from the beginning of the test. Thus, the TCA and CAA provide load carrying resistance simultaneously for UPPC frames. As the strands are unbonded, the TCA is dominant by the vertical component of prestressing forces. The contribution from CAA can be simply determined by subtracting the resistance of TCA from the measured load resistance. Fig. 12 illustrates the decomposition of the load resistance. It can be found that the CAA can even lead to negative contribution when MJD beyond one beam depth as the direction of vertical component of the arching force changes from upward to downward (refer to Fig. 11b) when the MJD is larger than one beam depth. For conventional RC frames, the TCA due to stretching of longitudinal reinforcements kicks in after vanish of CAA due to concrete crushing.

4. Dynamic test results

As mentioned above, to fully understand the dynamic response of UPPC frames subjected to sudden column removal and compare the static and dynamic behavior of UPPC frames, two dynamic specimens: UPPC-DL and UPPC-DH were dynamically tested under sudden column removal scenario. As mentioned above, a total of about 8400 kg weights (steel assemblies) were hung below the double-span beam before removal of the SCRD. As a result, an initial axial force of 40.5 kN and 40.2 kN were measured at the SCRD for UPPC-DL and UPPC-DH, respectively. The key results such as the maximum middle joint displacement and maximum horizontal compressive/tensile force were tabulated in Table 4. More detail discussion on dynamic response could be found as below.

4.1. Reliability of SCRD

To capture realistic dynamic response, the duration of column removal must be less than 10 % of the natural period of the vibration of the remaining frame [13]. Fig. 13 gives the varying of axial force in SCRD. As shown in the figure, for UPPC-DL, the initial axial force was 40.5 kN before column removal at a time of 0.01 s and it reduced to 0.0 kN at a time of 0.018 s. Thus, the duration was 0.008 s, which is about 1.1 % of its natural period of vibration. Similarly, the duration of UPPC-DH was 0.005 s, which is about 0.9 % of its natural period. Thus, the reliability of the SCRD was ensured.

4.2. Dynamic displacement responses

Figs. 14a and b illustrate the displacement response of UPPC-DL and UPPC-DH, respectively. For UPPC-DL, the maximum MJD is 320 mm at a time of 2.1 s. The maximum displacement of VD1, VD2, VD3, VD4, VD5, and VD6 are 88 mm, 170 mm, 253 mm, 250 mm, 168 mm, and 86 mm, respectively. For UPPC-DH, the maximum MJD is 295 mm a time of 1.99 s. The maximum displacement of VD1, VD2, VD3, VD4, VD5, and VD6 are 76 mm, 160 mm, 235 mm, 230 mm, 153 mm, and 73 mm, respectively. The deformation shape of the double-bay beam is shown in Fig. 15. It can be found that the beams keep straight at maximum MJD, which is similar to that of static tests.

Fig. 16 shows the horizontal displacement of the side columns of UPPC-DH. For exterior side column, the maximum outward horizontal displacements of LHD1, LHD2, LHD3, LHD4, and LHD5 (refer to Fig. 16a) are -1.88 mm, -1.01 mm, -2.36 mm, -1.57 mm, and -0.23 mm, respectively. While the maximum inward horizontal displacements are 3.97 mm, 4.62 mm, 5.18 mm, 4.27 mm and 3.12 mm, respectively. For interior side column, the maximum outward horizontal displacement of RHD1, RHD2, RHD3, RHD4, and RHD5 (refer to Fig. 16b) are -0.49 mm, -0.81 mm, -1.15 mm, -0.73 mm, and -0.46 mm, respectively, whereas the maximum inward horizontal displacement are 2.08 mm, 1.88 mm, 2.43 mm, 2.05 mm, and 1.01 mm, respectively. Therefore, similar to static tests, the exterior side column experiences larger horizontal deformation than that of interior one. In general, similar results are recorded in UPPC-DL.

4.3. Crack pattern and local damage

The crack pattern and local damage of UPPC-DL and UPPC-DH are illustrated in Figs. 17 and 18, respectively. The differences caused by different axial compression ratio are mainly reflected in the crack pattern of the side columns. It could be found that the cracks observed in the side columns of UPPC-DH are much fewer than that in UPPC-DL. Moreover, the cracks formed in the interior column are milder than that in the exterior one for both specimens. Compared with their static counterparts, UPPC-DL and UPPC-DH experiences similar damage at the similar displacement stage (refer to Figs. 19 and 20). Therefore, it was confirmed that the dynamic effects will not change the crack pattern and failure mode significantly. And the static push-down tests, which are most commonly experimental method for progressive collapse studies, are able to equivalently investigate the dynamic behavior of UPPC frames properly in terms of crack pattern and failure mode.

4.4. Horizontal reaction force

Fig. 21 illustrates the total horizontal reaction force at each side of tested specimens. For exterior side (without overhanging beam) of UPPC-DL, 1.0 s after suddenly removal of the column, total horizontal reaction force reaches maximum compressive force of -71 kN a time of 1.388 s, but then the compressive reaction force begins to decrease. At 1.71 s, the horizontal reaction force changes from compressive to tensile. The maximum tensile force of 110 kN is measured at a time of 2.15 s. After vibration, the residual force of 89 kN is measured. For interior side (with overhanging beam), the maximum horizontal compressive and tensile force are measured to be -84 kN and 185 kN at times of 1.323 s and 1.97 s, respectively. Therefore, similar to static ones, the interior side achieves larger compressive and tensile reaction force due to stronger horizontal restraints. For UPPC-DH, the maximum horizontal compressive force at exterior side and interior side are -75 kN and -96 kN, respectively, whereas the maximum horizontal tensile forces are 104 kN and 148 kN, respectively. Therefore, both CAA and TCA are also measured in dynamic tests, which confirm that dynamic effects will not change the load resisting mechanism of UPPC frames significantly. Moreover, it should be noted that although sudden column removal tests are investigated in literature [36-38], measuring dynamic horizontal reaction force after sudden column removal was very little.

Fig. 22 illustrates the contribution of each horizontal restraint to the total horizontal reaction force. For exterior side of UPPC-DH, as shown in Fig. 22a, the bottom pin support contributes majority of the compression force whereas the contribution from top roller is marginal. In tensile phase, the contribution of tensile reaction force from top roller is similar to that from bottom pin support. For the interior side, as shown in Fig. 22b, similar to the observation measured from the exterior side, the bottom pin support contributes the majority of the compression force. However, in tensile phase, the overhanging beam contributes the majority of the tensile force. In general, similar trends are measured for UPPC-DL.

5. Comparison of dynamic and quasi-static reaction force and prestressing force

Fig. 23 compares the total horizontal reaction force from dynamic and quasi-static tests. For UPPC-DL, the E-MHCF and I-MHCF are -71 kN and -84 kN, respectively. For UPPC-SL, the E-MHCF and I-MHCF are -62 kN and -75 kN, respectively. In tension phase, when the UPPC-DL (refer to Fig. 23a) reaches maximum displacement, the measured E-MHTF and I-MHTF are 110 kN and 185 kN, respectively. For static specimen UPPC-SL, at the same displacement, the E-MHTF and I-MHTF are 103 kN and 164 kN, respectively. As to UPPC-DH (refer to Fig. 23b), the E-MHCF, I-MHCF, E-MHTF, and I-MHTF are -75 kN, -96 kN, 104 kN, and 148 kN, respectively. For static specimen UPPC-SH, the E-MHCF, I-MHCF, E-MHTF, and I-MHTF are -67 kN, -84 kN, 92 kN, and 130 kN, respectively. Therefore, compared to static tests, the dynamic tests increase the horizontal reaction force up by 15 % and 14 % for compressive and tensile phases, respectively. The DIF for horizontal reaction force is up to 1.15.

Fig. 24 compares the total prestressing force from dynamic and quasi-static tests. The total initial prestressing force of UPPC-DL, UPPC-DH, UPPC-SL, and UPPC-SH are 242 kN, 241 kN, 240 kN, and 238 kN, respectively. When the maximum MJD was reached, the prestressing forces of UPPC-DL and UPPC-DH are 322 kN and 318 kN, respectively. At the same MJD, the prestressing forces of UPPC-SL and UPPC-SH are 300 kN and 305 kN, respectively. Therefore, the increments of prestressing force in UPPC-SL and UPPC-SH are 25.0 % and 28.2 %, respectively, which are smaller than their dynamic counterparts (33.1 % and 32.0 % for UPPC-DL and UPPC-DH, respectively).

6. Analytical investigation

Due to complexity in construction, only two dynamic tests and two quasi-static tests were carried out in this study. To fully understand the dynamic response of UPPC frames and to predict their dynamic ultimate load capacity (DUL), a nonlinear single-degree-of-freedom (SDOF) model was developed. After validation, the SDOF model was also used to investigate the effects of applied load, no-zero initial condition, and damping ratio.

6.1. Development of the refined SDOF analytical model

Fig. 25 illustrates the refined SDOF model, which could consider the load resistance in declining phase well. The model consists of an equivalent mass (m_e) connected to a fixed boundary via a nonlinear spring ($k_e u(t)$) and viscous dashpot ($c_e \dot{u}(t)$). The SDOF model can be expressed as Eq. 2:

$$m_e \ddot{u}(t) + c_e \dot{u}(t) + k_e u(t) = P(t) - R(t) \tag{2}$$

where m_e is the equivalent mass; c_e is a damping coefficient; k_e is an effective stiffness; $P(t)$ is the applied load, and $R(t)$ is the vertical resistance measured by the load cell (Item 14 in Fig. 2b), which was installed at SCRD. Note that, the m_e, c_e, and k_e of each specimen adopted in the SDOF model are correlated to their load resisting function, which were obtained from quasi-static tests.

6.2. Determination of m_e

As the shape function of the specimen is given, the equivalent mass can be determined by Eq. 3:

$$m_e = \int m(x)\left[\psi(x)\right]^2 dx + \sum_i m_i \left[\psi(x_i)\right]^2 \qquad (3)$$

where *m(x)* is the distributed mass function; *ψ(x)* is the shape function; m_i is concentrated mass *i* at location *i,* and $\psi(x_i)$ is shape function value at location *i*.

6.3. Determination of effective stiffness

As mentioned above, the effective stiffness is determined by the load resisting function measured from quasi-static test. One of the most significant differences between the dynamic and quasi-static test is strain rate effect (materials). According to the discussion in section "Comparison of dynamic and quasi-static reaction", the strain rate effect of material in this study is insignificant. Thus, it is reasonable to predict the dynamic response of dynamic tested specimens based on the measured load resisting function from static tests.

Another challenge is to determine the effective stiffness in post-yield stage. Reviewing previous studies, it can be found that there are several prevalent approaches: 1. Sassani and Sagiroglu [27] proposed a bilinear load-displacement relationship and the declining phase were ignored; 2. Calvi et al. [39] suggested to use secant stiffness at maximum displacement to consider post-yield strength of the structure; 3. Yu and Guo [28] adopted tri-linear load function that is capable of considering the resistance in declining phase. To obtain more accurate prediction, a more precise five-linear load function was employed in this study to determine the effective stiffness.

The load resisting functions of UPPC-DL and UPPC-DH are given in Figs. 26a and b, respectively. As shown in the figure, the load resisting functions consist of five linear segments (O-A, A-B, B-C, C-D and D-E). As no obvious yield load was found, the stiffness in segment A-B was set equal to the secant stiffness at the FPL. Beyond FPL, a load yield platform was formed. Thus, a constant stiffness equal to secant stiffness at point B was used to represent segment A-B. Effective stiffness of segment B-C was set equal to the slope of the load-displacement curve between point B and C. Point C is the point at which the slope of the curve began to change significantly due to *P-Δ* effect. Stiffness at point D (SPL) and point E (drop by 20 % from the SPL) are set equal to their secant stiffness while the points located in CD and DE can be determined by interpolation. The effective stiffness of key points can be found in Table 5.

6.4. Effective damping coefficient c_e

As illustrated in Eq. 4, the effective damping coefficient is a function of damping ratio, effective stiffness, and effective mass.

$$c_e = 2\zeta\sqrt{k_e m_e} \tag{4}$$

The effective stiffness and effective mass are discussed above. Therefore, the main objective in this section is to determine the damping ratio (ζ). As illustrated in Fig. 27, based on the logarithmic decrement method, the damping ratios were determined as 12.5 % and 11.5 % for UPPC-DL and UPPC-DH, respectively. The adopted effective damping coefficient for each segment can be easily calculated by Eq. 4.

6.5. Applied load and vertical reaction measured in the SCRD

The steel weights would produce an equivalent concentrated load $P(t)$ at the column stub. Meanwhile, the load cell (Item 14 in Fig. 2b) embedded in the SCRD would measure a vertical reaction force $R(t)$ with same magnitude of $P(t)$. Fig. 25 illustrates the function of $P(t)$ and $R(t)$. $R(t)$ begins to reduce when the SCRD knocked down at a time of t_0 and reduce to zero when the SCRD and the column stub separate completely at a corresponding time of $t_0+\Delta t$. In general, for $R(t)$, a nonlinear reduction function may be more realistic. However, as the column removal duration Δt is quite small (0.008 s and 0.005 s for UPPC-DL and UPPC-DH, respectively), the assumption of linear reduction of $R(t)$ has little effect on analytical results.

6.6. Validation of SDOF model

Fig. 28 compares the analytical displacement response to the measured ones. The predicted maximum displacement of UPPC-DL and UPPC-DH are 344 mm and 318 mm at time of 2.09 s and 2.02 s, respectively, which were 107.6 % and 107.8 % of the measured one, respectively. Therefore, the analytical curves agree with the measured ones well in term of maximum MJD as well as corresponding time. However, the vibration after maximum MJD from the analytical curve is more significant than that from tests. Moreover, the residual displacement from analytical model is less than that from tests. This is because the effective stiffness of the model is determined based on the measured load resisting function from monotonic tests. However, repeated vibration is observed in the displacement response beyond the maximum MJD. Therefore, the proposed effective stiffness method cannot reflect the stiffness of the dynamic specimen in the vibration stage beyond the maximum MJD. It should be noted that, the maximum MJD is most important for evaluation of the vulnerability of a frame to resist progressive collapse [26, 28] and thus the accuracy of validated SDOF model was acceptable and the models were utilized for further parametric analysis.

6.7. Dynamic incremental analysis

Effect of applied load

In this section, the SDOF model was used to calculate the dynamic response of UPPC frame under different load levels to predict the DUL of the specimens. As illustrated in Fig. 29, UPPC-DL survived from an applied load (P in the legend) of 67 kN while failed to survived from 68 kN and thus, the DUL of UPPC-DL was 67 kN. Similarly, the DUL of UPPC-DH was 61 kN.

Considering the dynamic increase factor (DIF) as a force-based factor [19], it can be determined as follows:

$$DIF = \frac{SUL}{DUL} \tag{5}$$

where SUL and DUL are the static and dynamic ultimate load, respectively.

Thus, the DIF of UPPC-DL and UPPC-DH are 1.34 and 1.28, respectively.

Effect of non-zero initial condition

If progressive collapse is triggered by extreme loading (e.g., gas explosions, impacts, vehicular collisions or terrorist attacks), it always accompanied by a non-zero initial condition like non-zero initial velocity and non-zero initial displacement. It is necessary to investigate the effect of non-zero initial condition on the dynamic response.

Fig. 30 shows the dynamic response of UPPC-DH under different initial velocities. With initial velocity of 0.5 m/s and -0.5 m/s, the maximum MJDs of UPPC-DH are determined as -342 mm and -343 mm, respectively. Further increase the initial velocity to 0.75 m/s and -0.75 m/s, the maximum MJDs are calculated as -371 mm and -376 mm, respectively. Therefore, both upward (positive value) and downward (negative value) initial velocities will increase the maximum MJD, which can be attributed to the additional kinematic involved.

Fig. 31 compares the MJD-time curves of UPPC-DH under different initial displacements. It can be found that, when the initial upward (positive value) displacements of 50 mm and 100 mm are given, the maximum MJDs are obtained as -340 mm and -362 mm, respectively. Thus, the initial upward initial displacement will increase the maximum MJD. This is because the additional strain energy due to initial upward displacement must be dissipated by the increased strain energy caused by downward displacement. In contrast, the downward (negative value) initial displacement will decrease the maximum MJD, as shown in the figure, with initial downward displacements of -50 mm and -100 mm, the maximum MJDs reach -306 mm and -287 mm, respectively.

Effect of damping ratio

The effective of additional damper in resisting earthquake has been investigated extensively. However, its merit in resisting progressive collapse attracted fewer attentions. Fig. 32 shows the effect of damping ratio on the maximum MJD. As shown in the figure, under a given applied load of 40 kN, the maximum MJDs are -354 mm, -326 mm, -303 mm, and -285 mm, respectively, with corresponding damping ratio of 5 %, 10 %, 15 %, and 20 %, respectively. The absolute value of the maximum MJD is decreased by 19.5 % when the damping ratio increased from 5 % to 20 %. Therefore, the benefits from large damping for mitigating progressive collapse are noticeable. Additional dampers, which employed to resist earthquake was also effective for resisting progressive collapse.

Comparison of the results from SDOF model and energy-based method

Energy-based method by Izzuddin et al. [25], is a simplified method to predict dynamic resistance. Compared to SDOF model, the energy-based method may achieve conservative results due to ignored damping effects. According to its assessment framework, the energy-based method is mathematically expressed as:

$$P_{CC}(u_d) = \frac{1}{u_d}\int_0^{u_d} P_{NS}(u)du \quad (6)$$

where $P_{CC}(u)$ and $P_{NS}(u)$ are the dynamic load resistance curve and static load resistance at the displacement demand u, respectively.

As shown in Fig. 33, the DUL calculated by energy-based method are 55 kN and 53 kN, respectively, for UPPC-SL and UPPC-SH. Based on SDOF model, the DUL of UPPC-SL and UPPC-SH are 67 kN and 61 kN, respectively. Therefore, for UPPC-SL and UPPC-SH, the DULs obtained from SDOF model are higher than that from energy-based method by 21.8 % and 15.1 %, respectively.

7. Conclusions

In this paper, a comparative study on experimental tests of four UPPC frames under quasi-static and dynamic loading regimes are performed to investigate the progressive collapse capacity of UPPC frames subjected to a penultimate column removal scenario. Moreover, a refined SDOF model was developed in this research and validated. Then, it was used to conduct dynamic incremental analysis. Based on experimental results and discussion, the following conclusions can be drawn:

1. The failure modes of UPPC frames are quite similar in both quasi-static and dynamic test. However, they are quite different to that of RC frames mainly due to discontinuous beam reinforcements. Therefore, no plastic hinges were formed at the beam ends whereas wide openings were concentrated at the beam-column interfaces. The damage of beam was concentrated at compressive toes but no cracks occurred along the beam. When a penultimate column was assumed to be lost, the failure of UPPC frame was controlled by large eccentric compressive failure in the exterior side column.
2. For dynamic tests, specimens with higher axial compression ratio experienced much milder damage. For quasi-static tests, higher axial compression ratio could increase the first peak load

slightly. However, it resulted in greater P-Δ effect at large deformation stage, which may result in pre-mature failure with less deformation capacity and second peak load.

3. The reliability of the column removal apparatus was proved to be satisfactory. The column removal durations were 0.008 s and 0.005 s for UPPC-DL and UPPC-DH, respectively, which well satisfied the requirements of DoD [13] that the column removal duration should be less than 1/10 of the natural period of the vibration.
4. Large damping ratio was demonstrated to have noticeable benefits in resisting progressive collapse. Non-zero initial velocity and initial upward displacement would increase the maximum dynamic displacement whereas initial downward displacement would decrease the maximum dynamic displacement. The dynamic increase factor of UPPC-DL and UPPC-DH were determined to be 1.34 and 1.28, respectively. However, for horizontal reaction force, the maximum dynamic increase factor was 1.15. Therefore, the dynamic increase factor was different even in a single dynamic test when different response was focused on.
5. Compared to the SDOF model, it was validated that the energy-based assessment framework proposed by Izzuddin et al. [24] predicted a more conservative dynamic progressive collapse resistance of UPPC frames due to ignored damping effects.

Acknowledgements

The authors gratefully acknowledge the financial support provided by the Natural Science Foundation of China (Nos. 51778153, 51568004, 51478118). Any opinions, findings and conclusions expressed in this paper do not necessary reflect the view of Natural Science Foundation of China.

References

[1] Priestley MJN. Overview of the PRESSS research program. PCI J 1991; 36(4):50-57.

[2] Stone WC, Cheok GS, Stanton JF. Performance of hybrid moment-resisting precast beam-column concrete connection subjected to cyclic loading. ACI Struct J 1995; 92(2):229–49.

[3] Stanton J, Stone WC, Cheok GS. A hybrid reinforced precast frame for seismic regions. PCI J 1997; 42(2):20–32.

[4] Morgen BG, Kurama YC. A friction damper for post-tensioned precast concrete moment frames. PCI J 2004; 49(4):112-32.

[5] Li L, Mander JB, Dhakal RP. Bi-directional cyclic loading experiment on a 3-D beam-column joint designed for damage avoidance, J Struct Eng 2008; 134(11):1733–42.

[6] Solberg KM, Dhakal RP, Bradley BA, Mander JB, Li L. Seismic performance of damage-protected beam–column joints. ACI Struct J 2008; 105(2):205–14.

[7] Bradley BA, Dhakal RP, Mander JB, Li L. Experimental multi-levels seismic performance assessment of 3D RC frame designed for damage avoidance. Earthquake Eng and Struct Dyn 2008; 37(1):1-20.

[8] Song LL, Guo T, Chen C. Experimental and numerical study of a self-centering prestressed concrete moment resisting frame connection with bolted web friction devices. Earthquake Eng Struct Dyn 2014; 43(4):529–45.

[9] Song LL, Guo T, Gu Y, Cao ZL. Experimental study of a self-centering prestressed concrete frame subassembly. Eng Struct 2015; 88:176–88.

[10] Song LL, Guo T, Gu Y, Cao ZL. Seismic response of self-centering prestressed concrete moment resisting frames with web friction devices. Soil Dyn Earthq Eng 2015; 71:151-62.

[11] Lu XZ, Zhang L, Lin KQ, Li Y. Improvement to composite frame systems for seismic and progressive collapse resistance. Eng Struct 2019; 186:227-42.

[12] Qian K, Liang SL, Fu F, Fang Q. Progressive collapse resistance of precast concrete beam-column sub-assemblages with high-performance dry connections. Eng Struct 2019; 198:109552.

[13] Department of Defense (DoD). Design of building to resist progressive collapse. Unified facility criteria, UFC 4-023-03, Washington, DC; 2010.

[14] Sadek F, Main J, Lew H, Bao Y. Testing and analysis of steel and concrete beam-column assemblies under a column removal scenario. J Struct Eng 2011; 137(9):881–92.

[15] Qian K, Li B. Performance of three-dimensional reinforced concrete beam-column substructures under loss of a corner column scenario. J Struct Eng 2013; 139(4):584-94.

[16] Qian K, Li B. Slab effects on response of reinforced concrete substructures after loss of corner column. ACI Struct J 2012; 109:845-55.

[17] Yu J, Tan K H. Structural behavior of reinforced concrete beam-column sub-assemblages under a middle column removal scenario. J Struct Eng 2013; 139(2):233-50.

[18] Valipour H, Vessali N, Foster SJ, Samali B. Influence of concrete compressive strength on the arching behaviour of reinforced concrete beam assemblages. Int J Adv Struct Eng 2015; 18(8): 1199-214.

[19] Quiel SE, Naito CJ, Fallon CT. A non-emulative moment connection for progressive collapse resistance in precast concrete building frames. Engineering Structures 2019; 179:174-188.

[20] Qian K, Li B. Dynamic performance of RC beam-column substructures under the scenario of the loss of a corner column—Experimental results. Eng Struct 2012; 42:154-67.

[21] Qian K, Li B. Quantification of slab influences on the dynamic performance of RC frames against progressive collapse. J Perform Constr Facil 2015; 29(1):04014029.

[22] Yu J, Rinder T, Stolz A, Tan K H, Riedel W. Dynamic progressive collapse of an RC assemblage induced by contact detonation. J Struct Eng 2014; 140(6):04014014.

[23] Russell JM, Owen JS, Hajirasouliha I. Experimental investigation on the dynamic response of RC flat slabs after a sudden column loss. Eng Struct 2015; 99:28-41.

[24] Qian K, Weng YH, Li B. Improving behavior of reinforced concrete frames to resist progressive collapse through steel bracings. J Struct Eng 2019; 145(2):04018248.

[25] Izzuddin B, Vlassis A, Elghazouli A, Nethercot D. Progressive collapse of multistorey buildings due to sudden column loss-Part I: Simplified assessment framework. Eng Struct 2008; 30:1308–18.

[26] Tsai MH. An analytical methodology for the dynamic amplification factor in progressive collapse evaluation of building structures. Mech Res Commun 2010; 37(1):61–66.

[27] Sasani M, Sagiroglu S. Progressive collapse of reinforced concrete structures: A multihazard perspective. ACI Struct J 2008; 105(1):96–103.

[28] Yu J, Guo YQ. Nonlinear SDOF model for dynamic response of structures under progressive collapse. J Eng Mech 2016; 142(3):04015103.

[29] ACI Committee 318, Building Code Requirements for Structural Concrete (ACI 318-14) and Commentary (318R-14). American Concrete Institute, Farmington Hills, MI, 433 pp; 2014.

[30] Su YP, Tian Y, Song XS. Progressive collapse resistance of axially-restrained frame beams. ACI Struct J 2009; 106(5):600–7.

[31] Yu J, Tan KH. Special detailing techniques to improve structural resistance against progressive collapse. J Struct Eng 2014; 140(3):04013077.

[32] Kang SB, Tan KH. Behaviour of precast concrete beam-column sub-assemblages subject to column removal. Eng Struct 2015; 93:85–96.

[33] Nimse RB, Joshi DD, Oatel PV. Behavior of wet precast beam column connections under progressive collapse scenario: an experimental study. Int J Adv Struct Eng 2014; 6(4):149–59.

[34] Al-Salloum YA, Alrubaidi MA, Elsanadedy HM, Almusallam TH. Strengthening of precast RC beam-column connections for progressive collapse mitigation using bolted steel plates. Engineering Structures 2018; 161:146-160.

[35] Zhou Y, Chen TP, Pei YL, Hwang HJ, Hu X, Yi WJ. Static load test on progressive collapse resistance of fully assembled precast concrete frame structure. Engineering Structures 2019; 200:109719.

[36] Sasani M. Response of a reinforced concrete infilled-frame structure to removal of two adjacent columns. Eng Struct 2008; 30(9):2478–91

[37] Sasani M, Sagiroglu S. Gravity load redistribution and progressive collapse resistance of 20-story reinforced concrete structure following loss of interior column. ACI Struct J 2010; 107(6):636–44.

[38] Sasani M, Kazemi A, Sagiroglu S, Forest S. Progressive collapse resistance of an actual 11-story structure subjected to severe initial damage. J Struct Eng 2011; 137(9):893–902.

[39] Calvi G M, Priestley M J N, Kowalsky MJ. Displacement-based seismic design of structures, IUSS Press, Pavia, Italy, 2008.

Table 1-Specimen information

Specimen ID	Element Size			span/depth ratio	Axial compression ratio	Effective prestress	Loading approach
	Span (mm)	Beam (mm×mm)	Column (mm×mm)				
UPPC-SL	2750	150×250	250×250	11	0.2	$0.65f_{pu}$	Static
UPPC-SH	2750	150×250	250×250	11	0.4	$0.65f_{pu}$	Static
UPPC-DL	2750	150×250	250×250	11	0.2	$0.65f_{pu}$	Dynamic
UPPC-DH	2750	150×250	250×250	11	0.4	$0.65f_{pu}$	Dynamic

Note: f_{pu} is the nominal ultimate strength of the unbounded post-tensioned strands (1860 MPa).

Table 2-Material properties

Item	Nominal diameter (mm)	Yield strength (MPa)	Ultimate strength (MPa)	Elastic modulus (MPa)	Elongation (%)
Stirrups R6	6	368	485	162,000	20.1
Beam reinforcements T12	12	462	596	171,000	14.7
Column reinforcements T16	16	466	604	182,000	17.0
Unbonded strands	12.7	1,649	1,970	213,000	6.3

Table 3- Definition of abbreviations

MJD	Middle Joint Displacement
MMJD	Maximum Middle Joint Displacement
FPL	First Peak Load
SPL	Second Peak Load
E-MHCF	Maximum Horizontal Compressive Force on Exterior Side
I-MHCF	Maximum Horizontal Compressive Force on Interior Side
E-MHTF	Maximum Horizontal Tensile Force on Exterior Side
I-MHTF	Maximum Horizontal Tensile Force on Interior Side
SUL	Static Ultimate Load
DUL	Dynamic Ultimate Load

Table 4-Test results

Specimen ID	FPL (kN)	SPL (kN)	E-MHCF (kN)	I-MHCF (kN)	E-MHTF (kN)	I-MHTF (kN)	MMJD (mm)
UPPC-SL	39	90	-62	-75	135	259	N/A
UPPC-SH	41	78	-67	-84	156	253	N/A
UPPC-DL	N/A	N/A	-71	-84	110	185	320
UPPC-DH	N/A	N/A	-75	-96	104	148	295

Note: FPL and SPL represent first peak load and second peak load, respectively; I-MHCF/I-MHTF and E-MHCF/E-MHTF represent maximum horizontal compressive /tensile force on interior and exterior side, respectively; MMJD represents maximum middle joint displacement

Table 5-Parameters in SDOF model and analytical results

Specimen ID	m_e (kg)	k_A (kN/m)	k_B (kN/m)	k_C (kN/m)	k_D (kN/m)	k_E (kN/m)	MMJD (mm)	DUL	$\frac{SUL}{DUL}$
UPPC-DL	18006	1258	150	190	152	106	344	67	1.34
UPPC-DH	18006	1367	165	222	169	107	318	61	1.28

Note: MMJD represents maximum middle joint displacement; DUL and SUL represent dynamic ultimate load and static ultimate load, respectively.

List of Figures

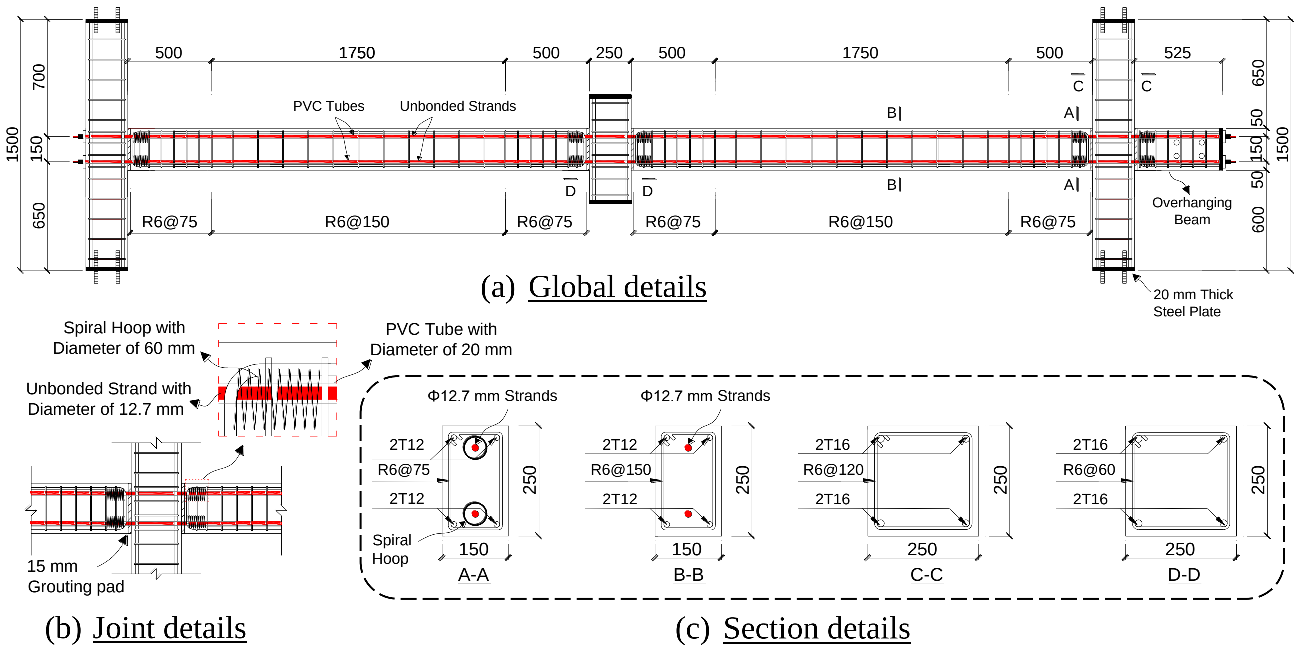

Fig. 1 Details of test specimen: (a) global details; (b) joint details; (c) section details

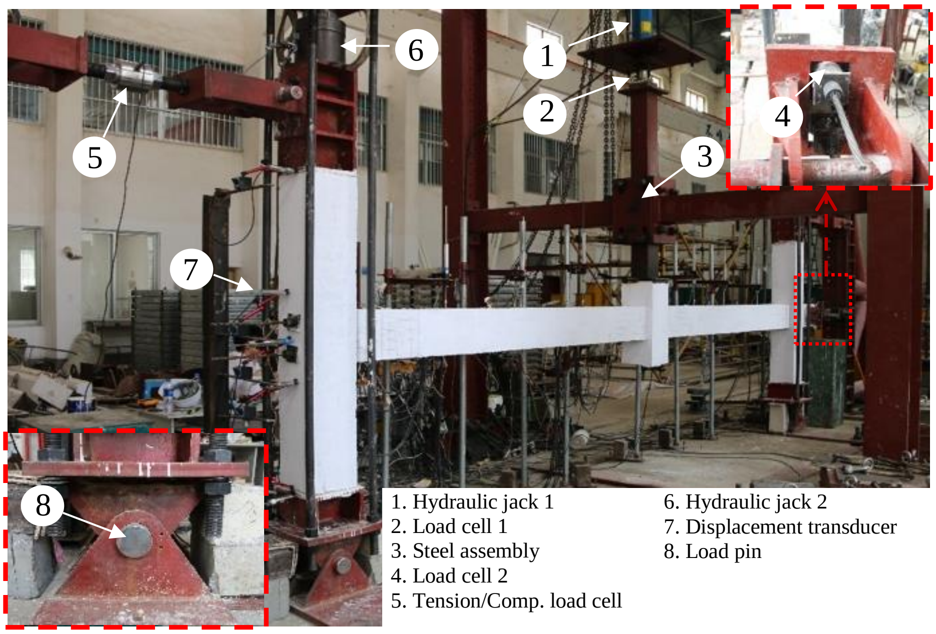

(a)

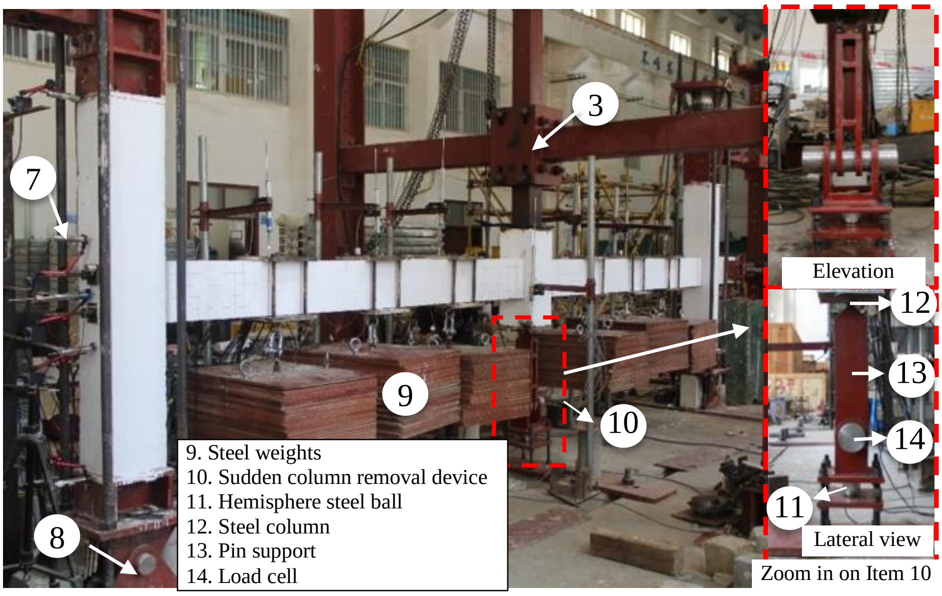

(b)

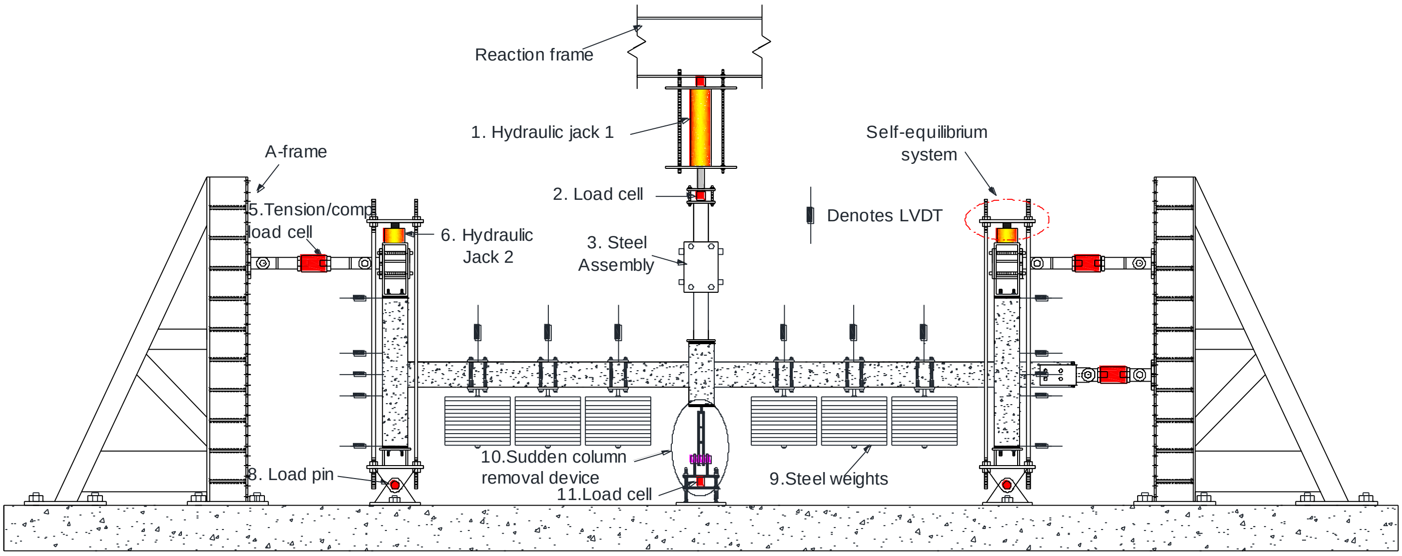

(c)

Fig. 2 Test setup: (a) quasi-static test-photo; (b) dynamic test-photo; (c) dynamic test-drawing

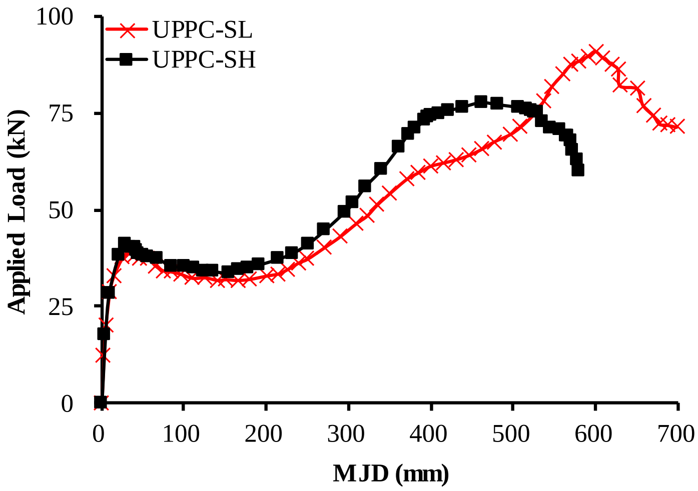

Fig. 3 Vertical load-displacement curves

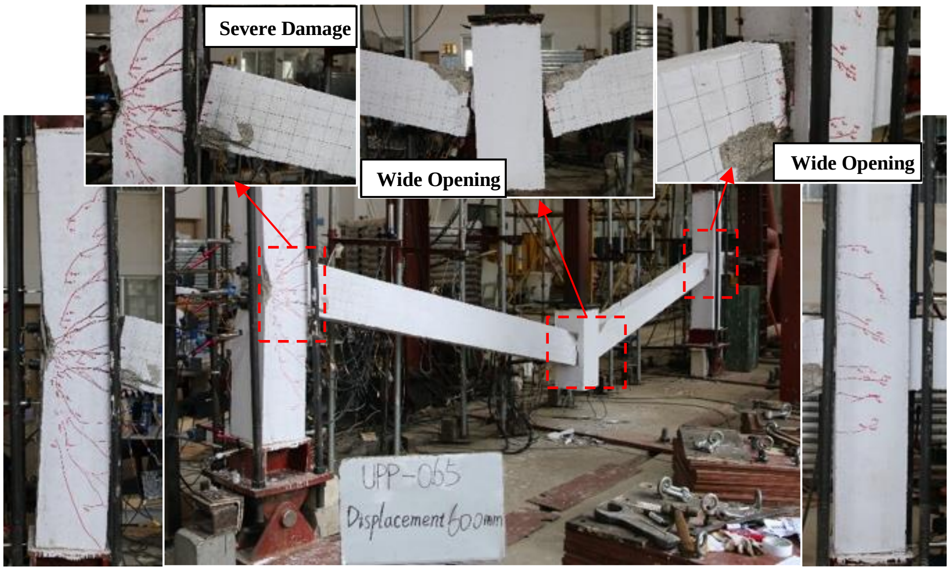

Fig. 4 Failure mode of UPPC-SL

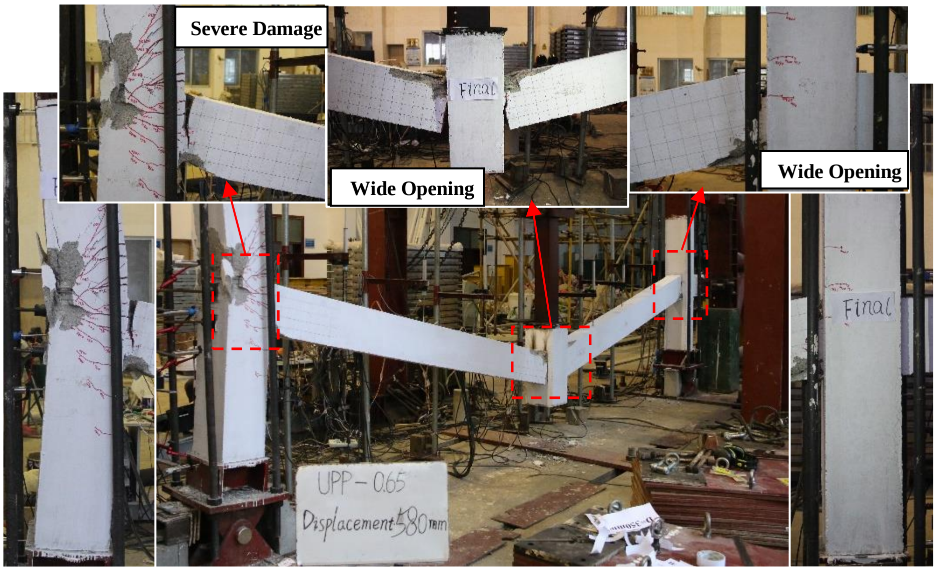

Fig. 5 Failure mode of UPPC-SH

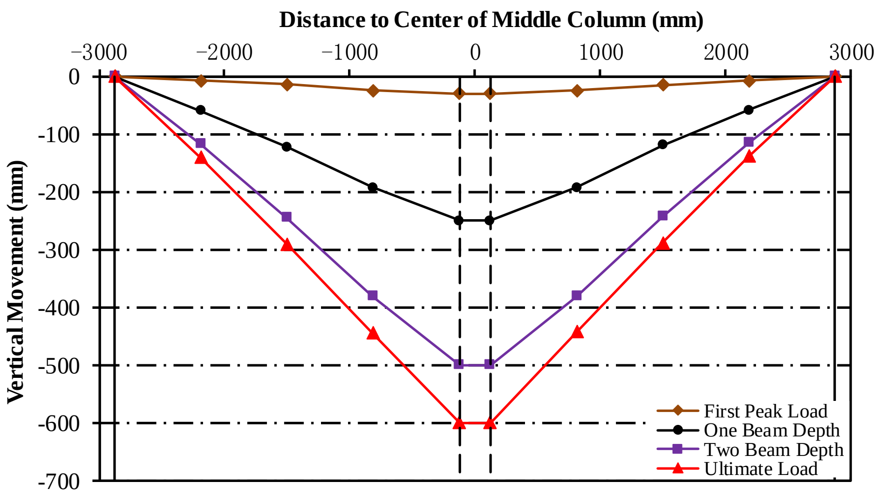

Fig. 6 Deflection of the double-bay beam of UPPC-SL

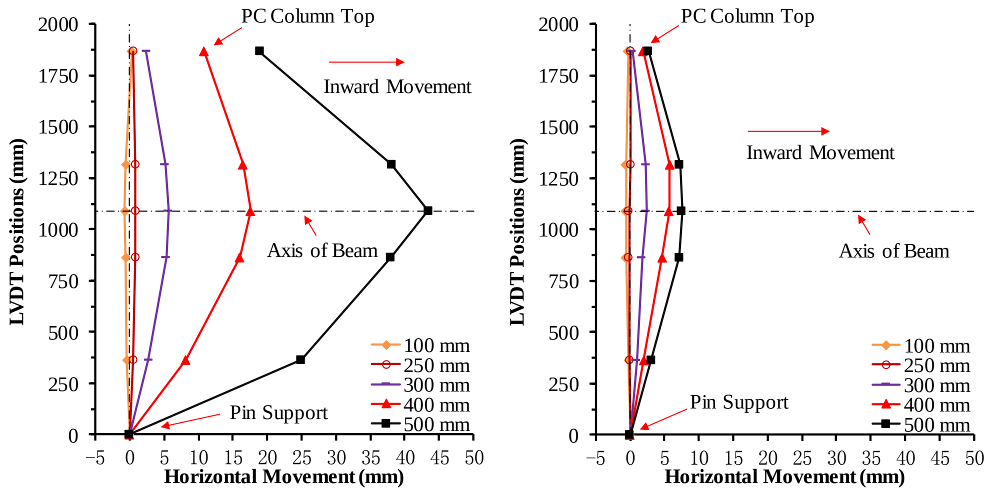

(a) (b)

Fig. 7 Horizontal drift in side columns of UPPC-HL: (a) exterior side column; (b) interior side column

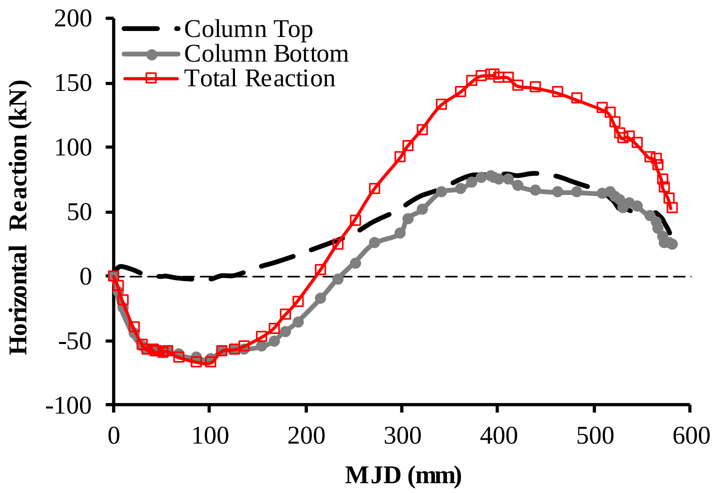

(a)

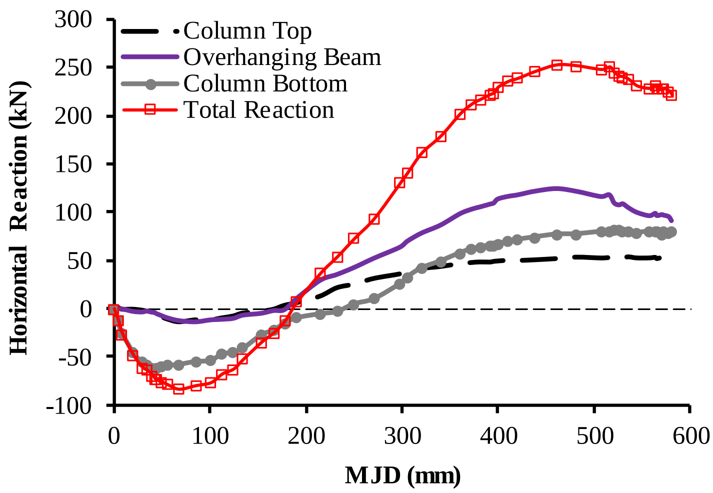

(b)

Fig. 8 Horizontal reaction of UPPC-SH: (a) exterior side; (b) interior side

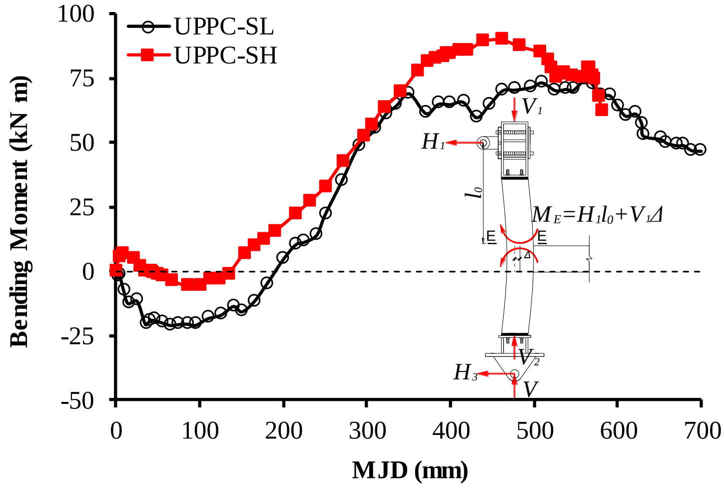

Fig. 9 Variation of bending moment in the exterior side column

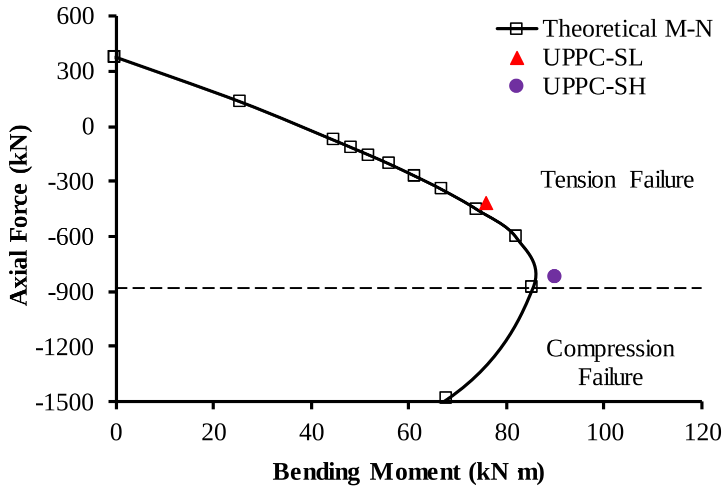

Fig. 10 Determination of the failure mode of the exterior side column

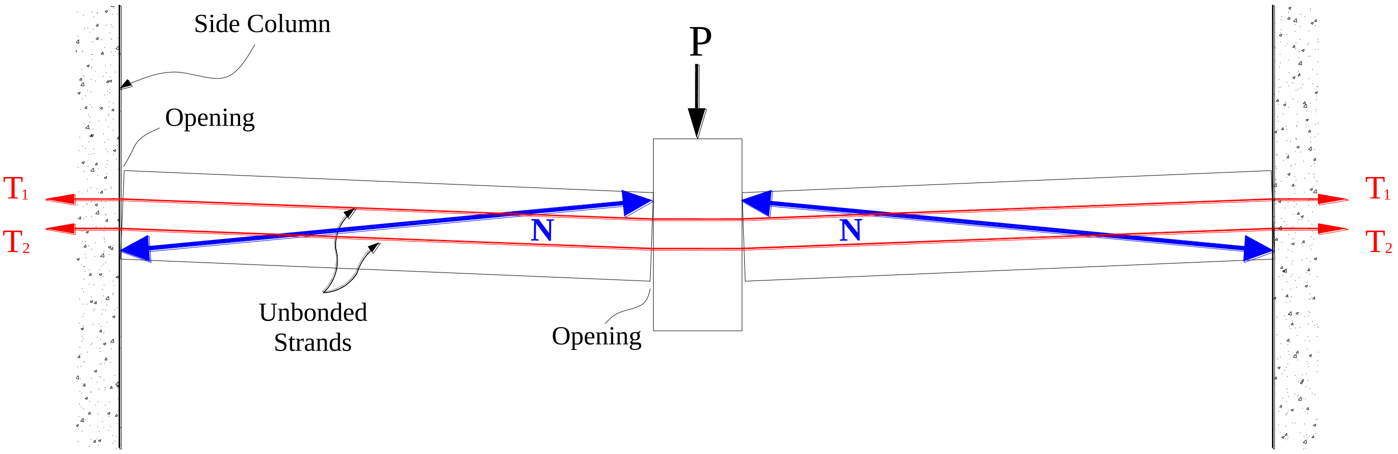

(a) MJD smaller than one beam depth

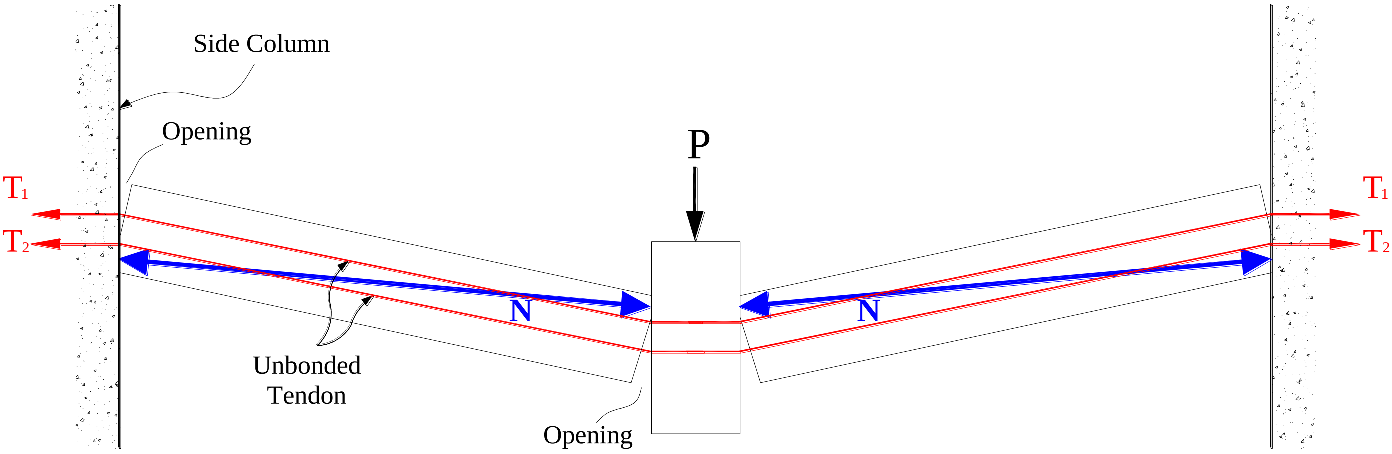

(b) MJD beyond one beam depth

Fig. 11 Load resisting mechanism in UPPC frame: (a) MJD smaller than one beam depth; (b) MJD beyond one beam depth

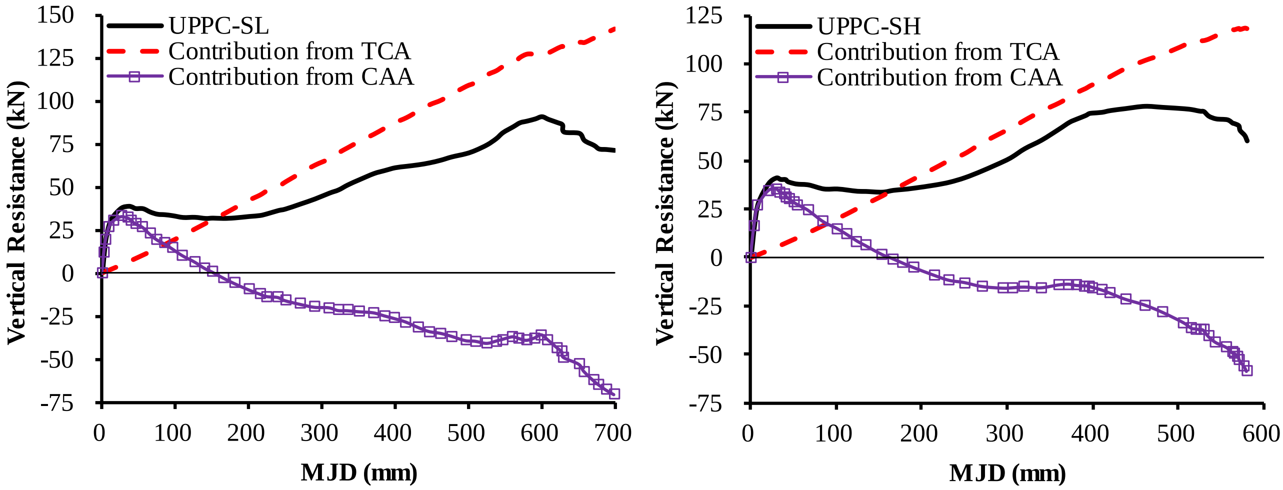

(a) UPPC-SL (b) UPPC-SH

Fig. 12 Load resistance decomposition of test specimens: (a) UPPC-SL; (b) UPPC-SH

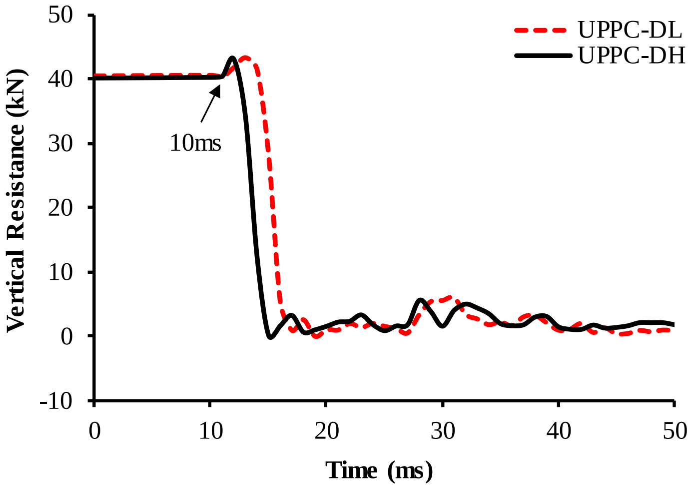

Fig. 13 Column removal duration

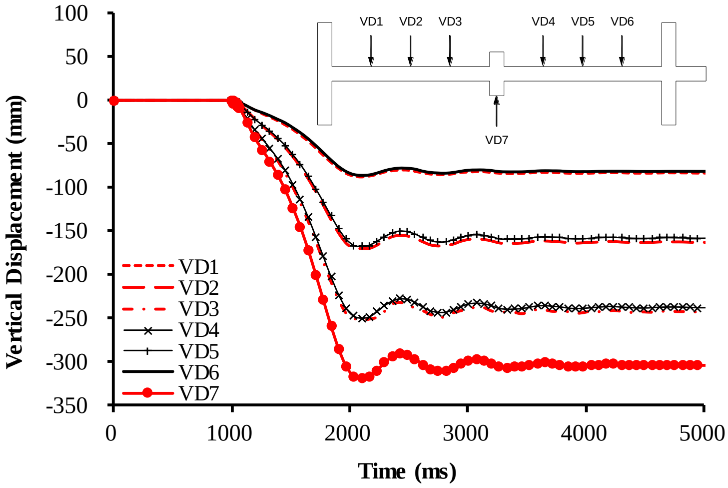

(a)

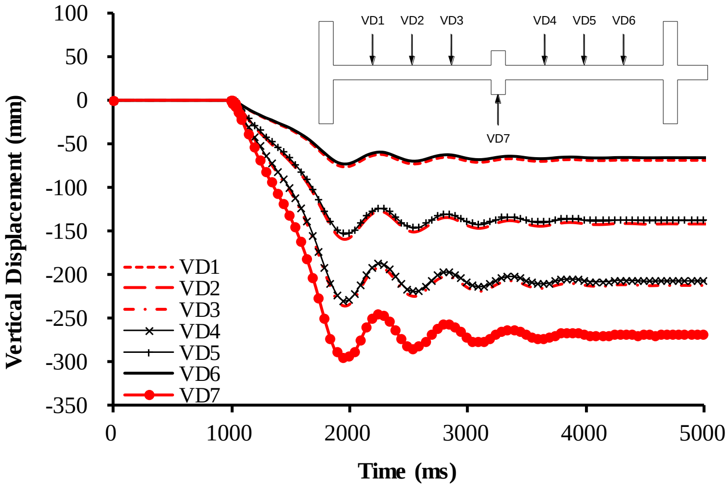

(b)

Fig. 14 Deflection of the double-bay beam: (a) UPPC-DL; (b) UPPC-DH

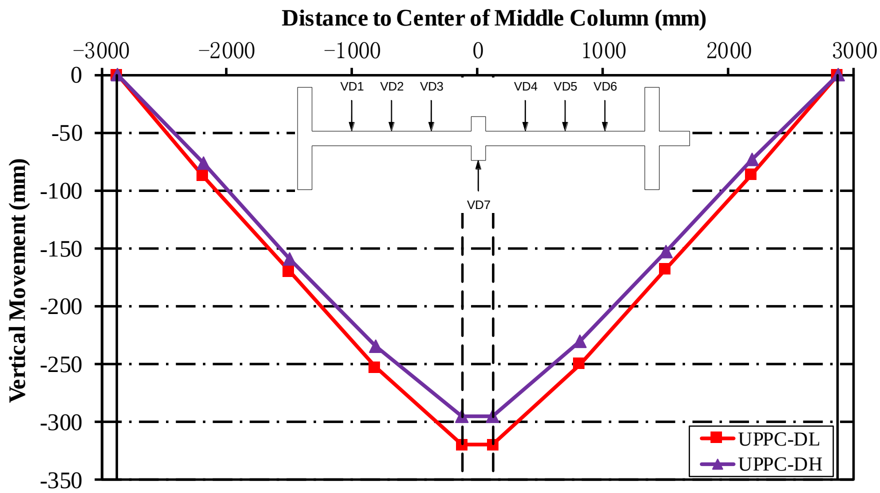

Fig. 15 Deformation shapes of the double-bay beam

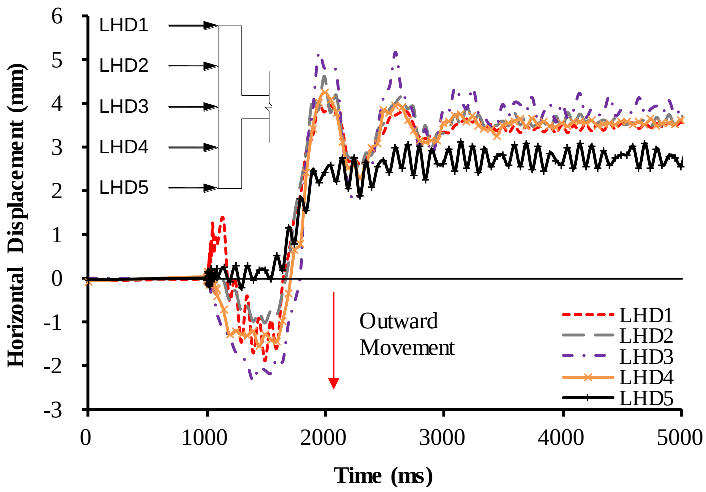

(a)

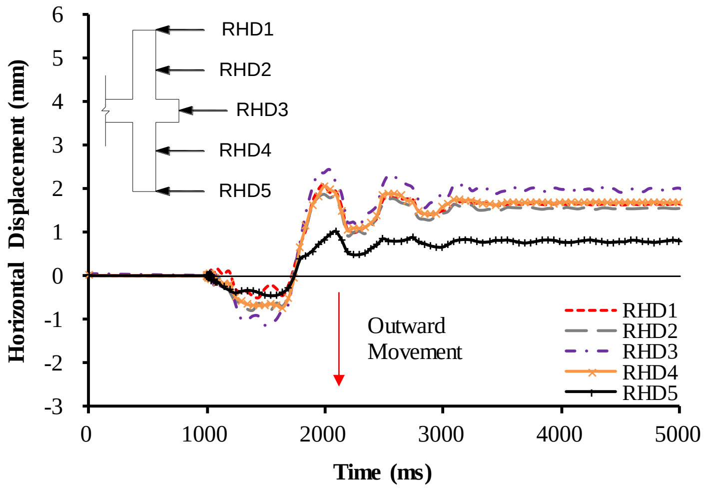

(b)

Fig. 16 Horizontal displacement in side column of UPPC-DH: (a) exterior side column; (b) interior side column

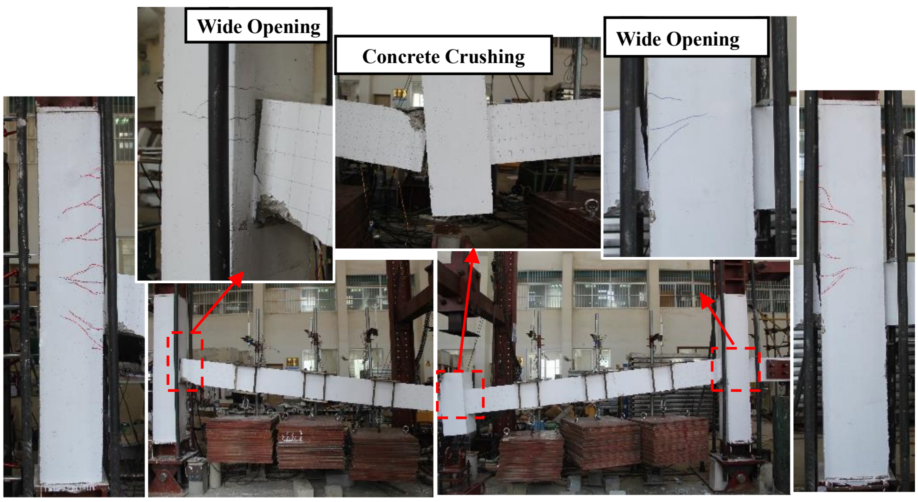

Fig. 17 Crack pattern and local damage of UPPC-DL

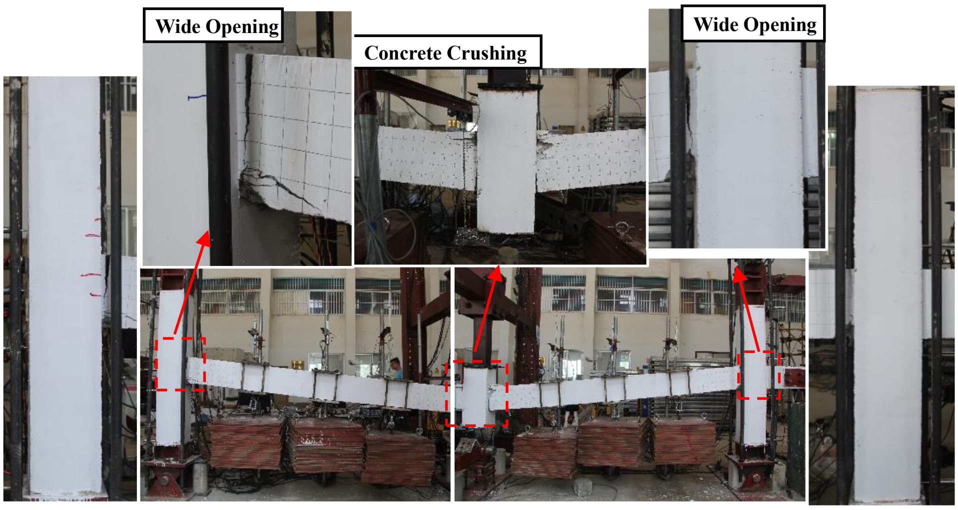

Fig. 18 Crack pattern and local damage of UPPC-DH

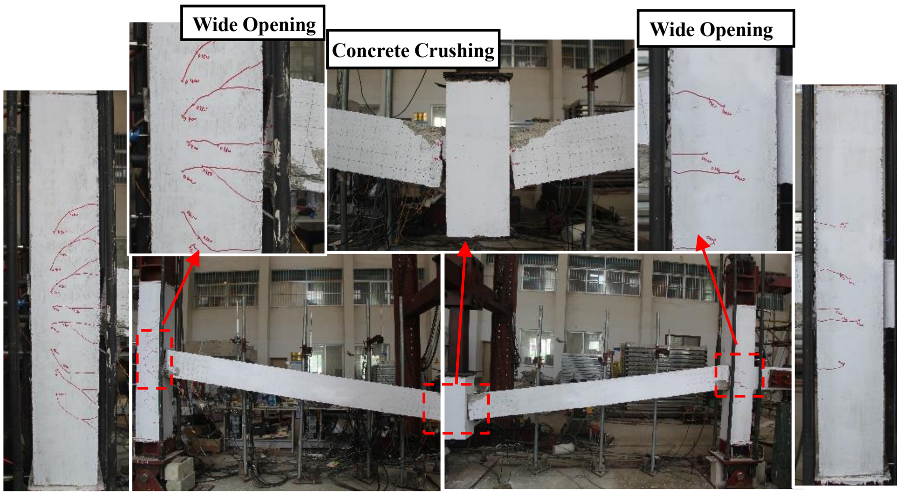

Fig. 19 Crack pattern and local damage of UPPC-SL at MJD of 320 mm

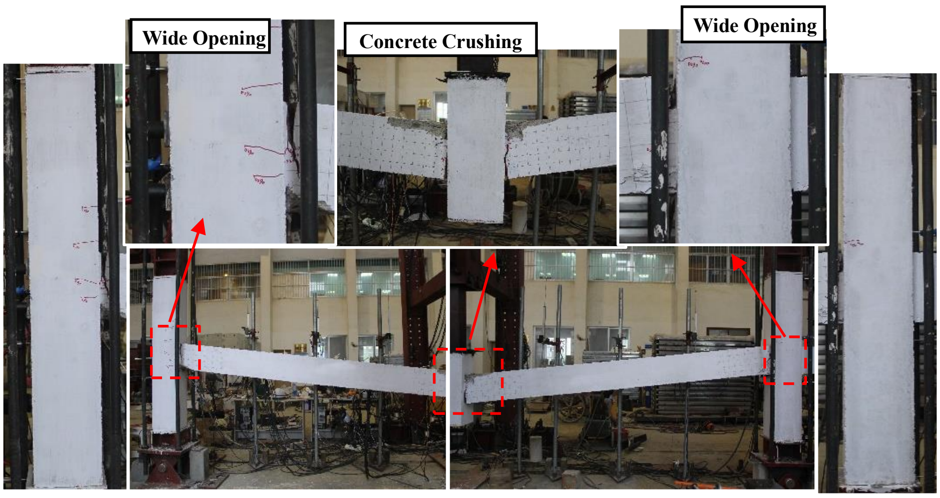

Fig. 20 Crack pattern and local damage of UPPC-SH at MJD of 295 mm

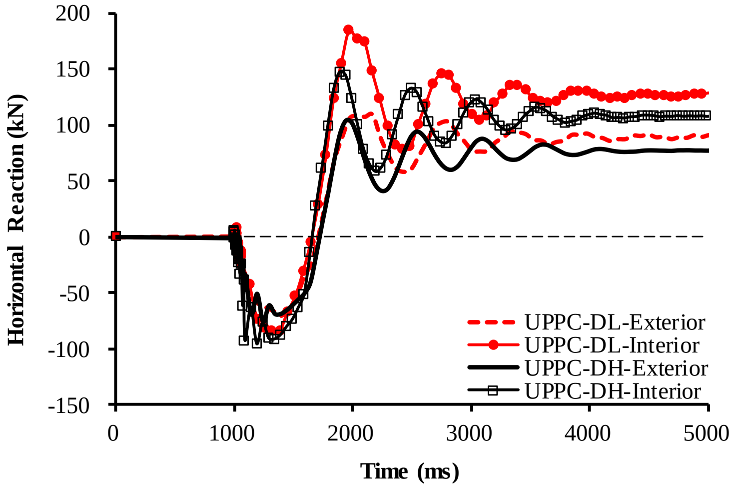

Fig. 21 Total horizontal reaction-time curves

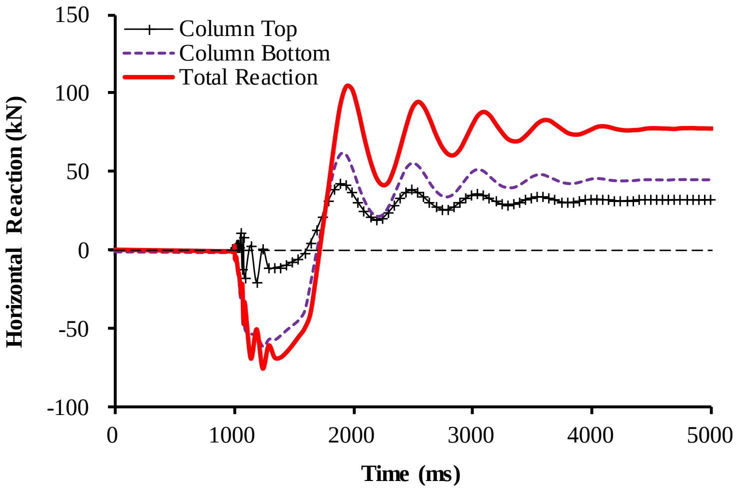

(a)

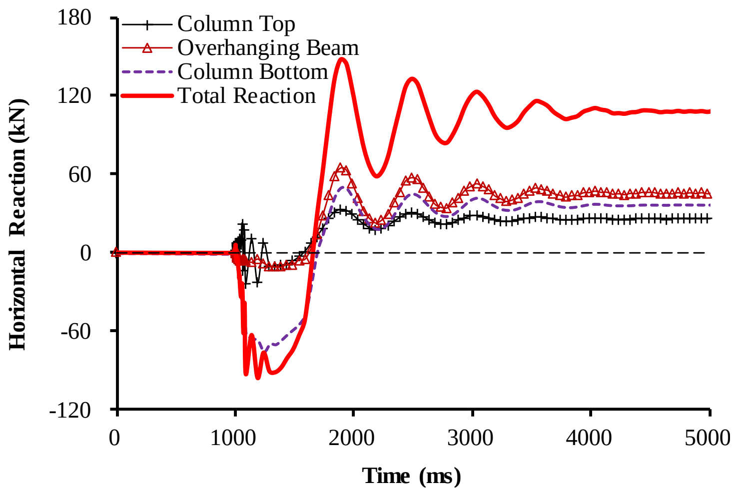

(b)

Fig. 22 Horizontal reaction of UPPC-DH: (a) exterior side; (b) interior side

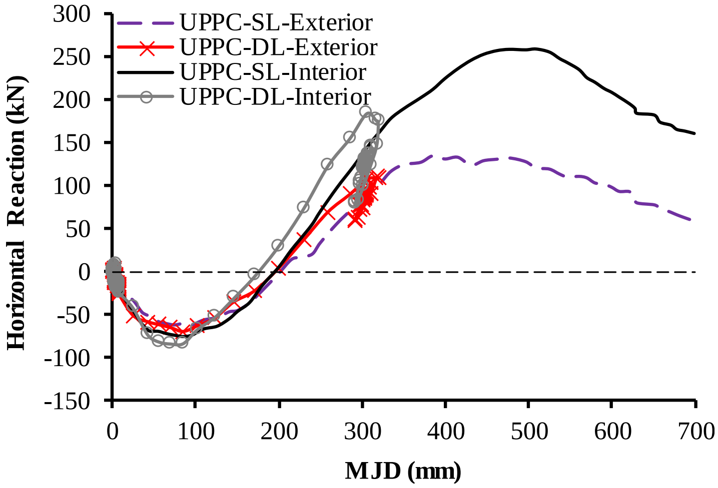

(a)

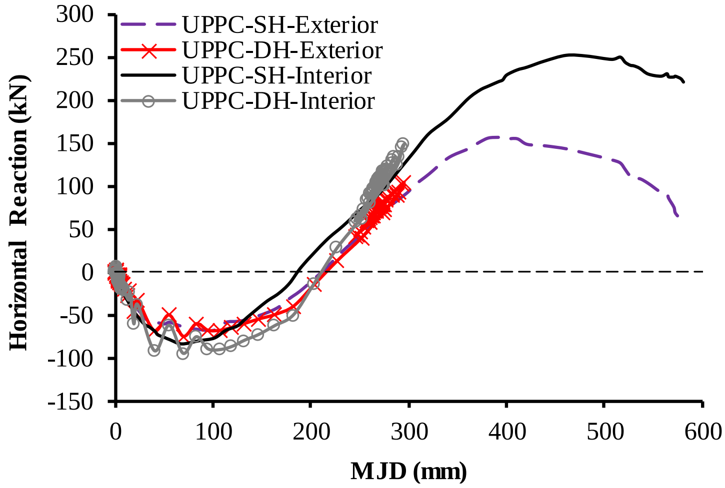

(b)

Fig. 23 Comparison of the total horizontal reaction: (a) UPPC-SL vs. UPPC-DL; (b) UPPC-SH vs. UPPC-DH

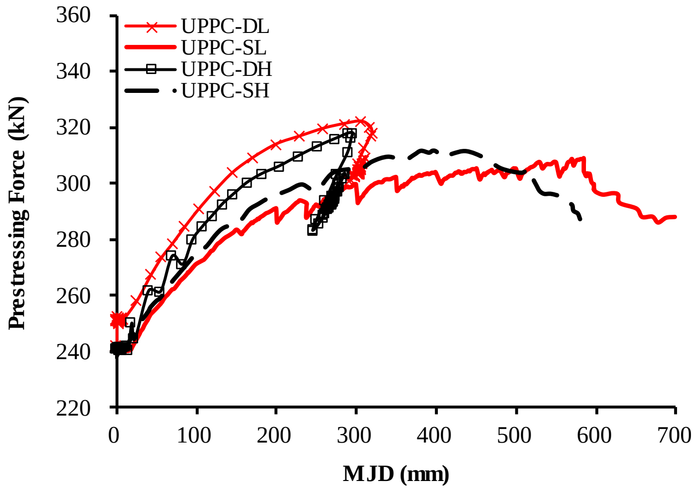

Fig. 24 Variation of prestressing forces in strands

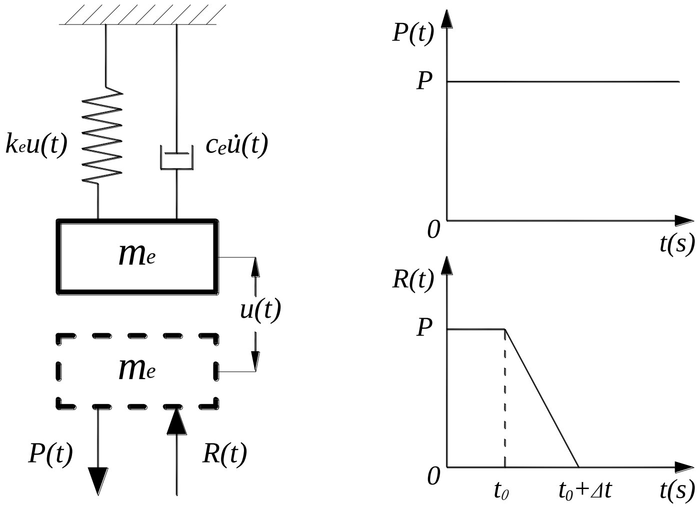

Fig. 25 Simplified SDOF model

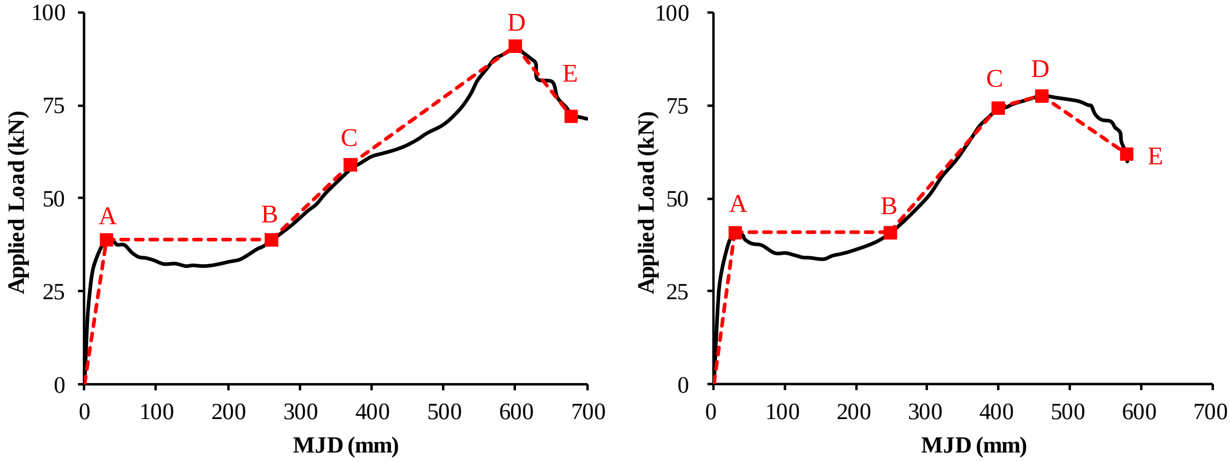

(a) (b)

Fig. 26 Load resisting function: (a) UPPC-SL; (b) UPPC-SH

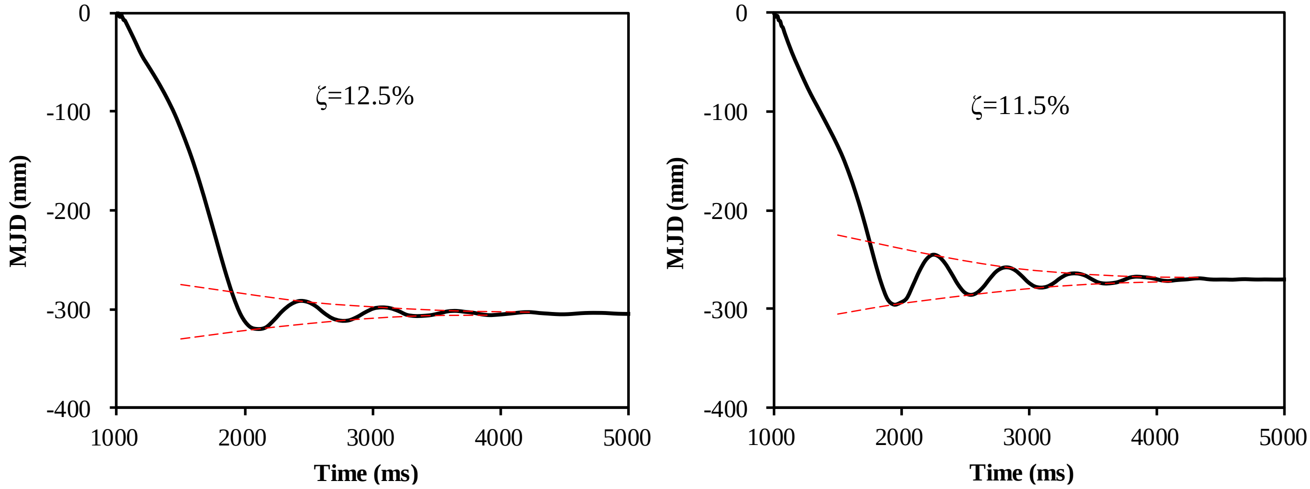

(a) (b)

Fig. 27 Determination of damping ratio: (a) UPPC-DL; (b) UPPC-DH

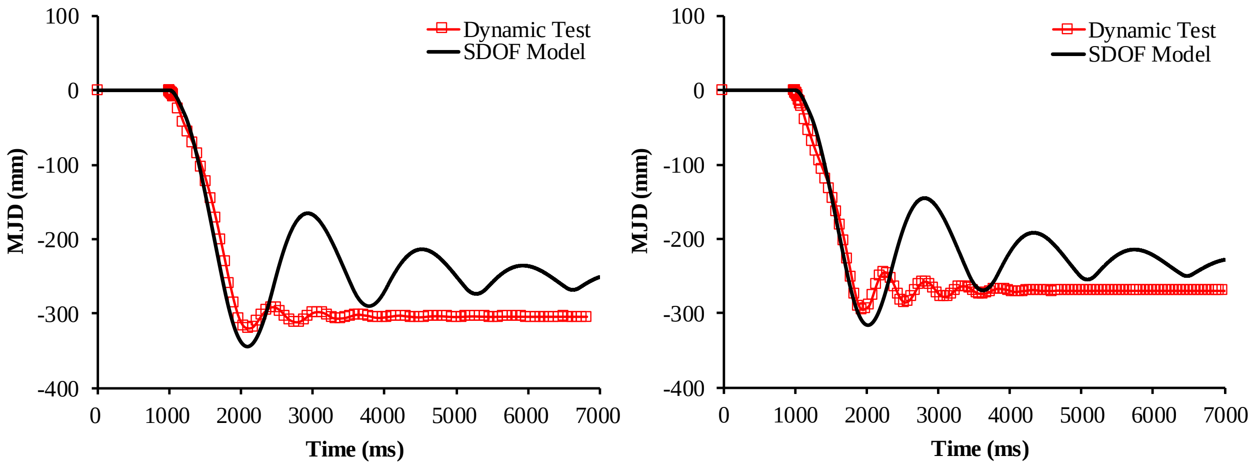

(a) (b)

Fig. 28 Comparison of the theoretical MJD to the measured one: (a) UPPC-DL; (b) UPPC-DH

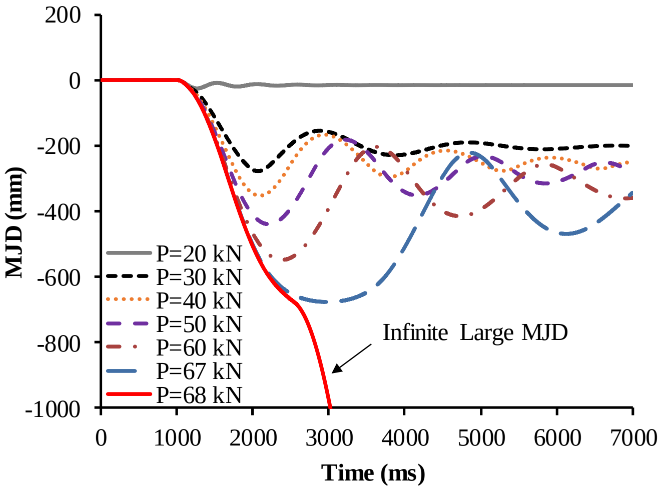

Fig. 29 Determination of dynamic ultimate load

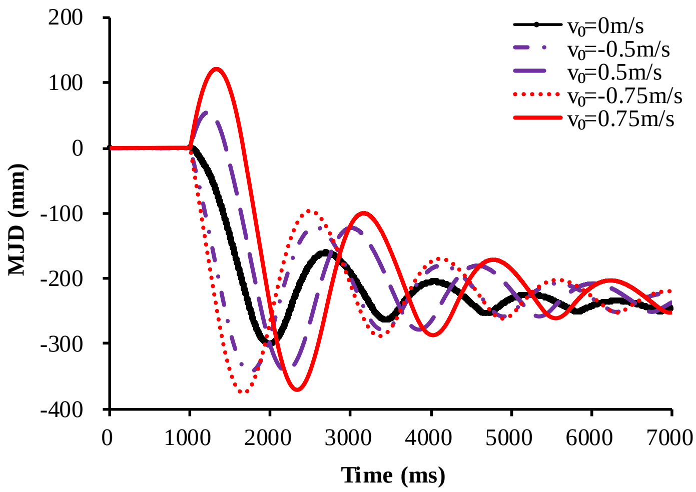

Fig. 30 Effect of initial velocity

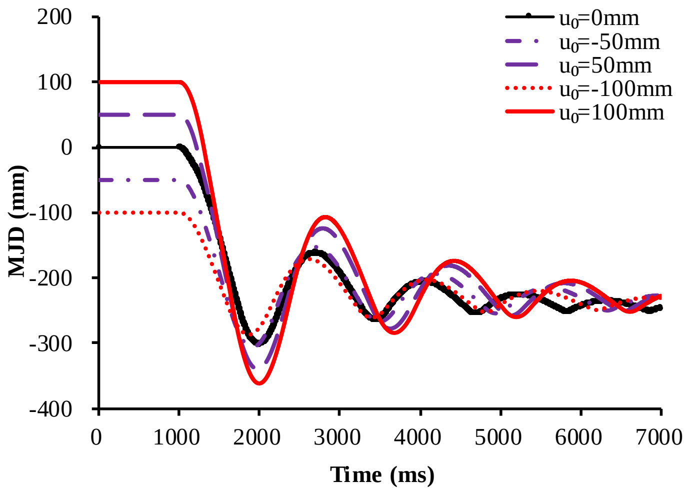

Fig. 31 Effect of initial displacement

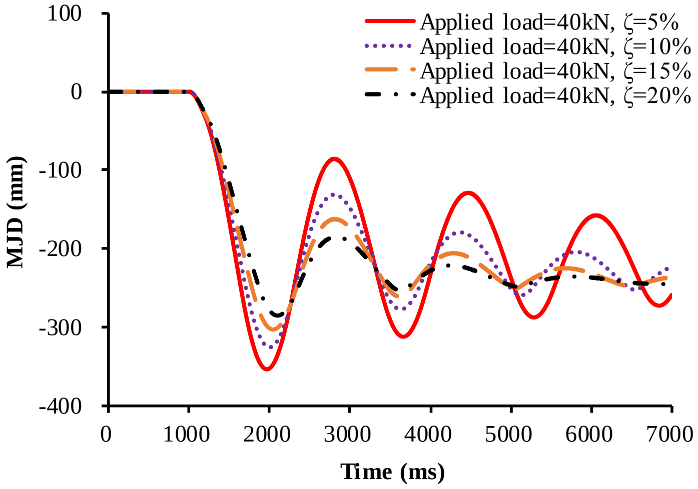

Fig. 32 Effect of damping ratio

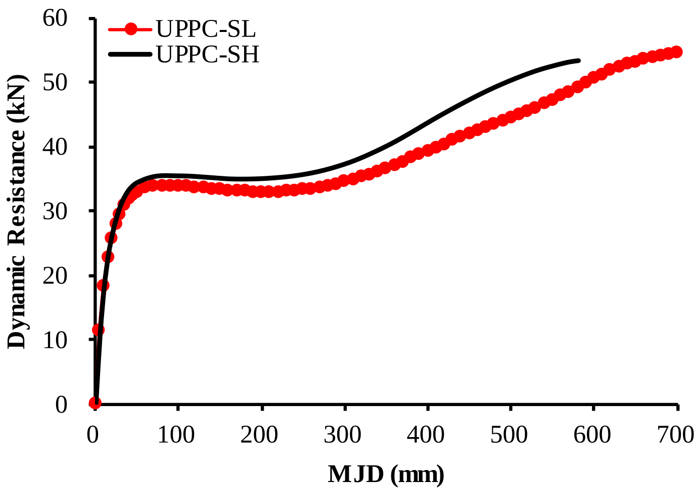

Fig. 33 Dynamic resistance based on energy method